

Evolution of coupled scalar perturbations through smooth reheating. II. Thermal fluctuation regime

M. Laine^a, S. Procacci^b, A. Rogelj^a

^a*AEC, Institute for Theoretical Physics, University of Bern,
Sidlerstrasse 5, CH-3012 Bern, Switzerland*

^b*Département de Physique Théorique, Université de Genève,
24 quai Ernest Ansermet, CH-1211 Genève 4, Switzerland*

Abstract

Curvature perturbations with short wavelengths exit the Hubble horizon when the universe may contain a thermal plasma in addition to an inflaton field that drives its expansion. We solve the corresponding fluctuation-dissipation dynamics at linear order, building upon a previously established set of gauge-invariant evolution equations. The properties of the noise autocorrelator are constrained via a matching of equilibrium correlators to quantum-statistical physics deep inside the Hubble horizon. The curvature power spectrum is determined numerically, without slow-roll approximations or assumptions about the equilibration of the inflaton field. As applications, we scrutinize two issues from recent literature: the model dependence of the thermally modified power spectrum as a function of freeze-out parameters, and the viability of embedding warm inflation within the Standard Model (we offer support for the latter proposal). The role of pre-horizon-exit acoustic oscillations is illustrated.

Emails: laine@itp.unibe.ch, simona.procacci@unige.ch, alica.rogelj@unibe.ch

Contents

1	Introduction	1
2	Evolution equations and initial conditions for perturbations	3
2.1	General set of gauge-invariant equations	3
2.2	Scale hierarchies and simplifications for the weak regime	7
2.3	Classical representation of the quantum-mechanical initial state	8
3	What an effective-theory perspective tells about the thermal noise	9
4	Numerical method for the stochastic evolution	15
5	Benchmarks and overall features	17
6	Can $\mathcal{P}_{\mathcal{R}}$ be expressed in terms of freeze-out parameters?	21
7	Testing a Standard Model embedded warm inflation scenario	25
8	Conclusions and outlook	27
A	Inflaton potential, radiation plasma, and background initial conditions	29

1. Introduction

New probes of the early universe can arise from precision measurements at larger momenta (smaller distance scales) than has been the norm in the past. Already now, the accuracy of the Planck CMB data [1] has been surpassed at angular momenta $\ell > 2000$ by new generations of terrestrial observatories [2], yielding improved constraints on the primordial power spectrum. Further data is arising from large-scale structure, notably with the forthcoming Euclid mission [3]. Information about the earliest halos [4] may require larger initial inhomogeneities than a straightforward extrapolation from the CMB domain would suggest. Future studies of gravitational waves will extend the sensitivity up to very high frequencies [5].

Within the inflationary paradigm, a given comoving momentum mode exits the Hubble horizon at an early time, and is then “frozen” for a long while, being insensitive to the physics that may be taking place at smaller distances. In a late universe, the mode re-enters inside the Hubble horizon, and is again susceptible to causal phenomena. Increasing the comoving momentum, a mode exits later, and re-enters earlier. Large momenta are therefore more sensitive to the physics that separates inflation and the radiation-dominated universe, referred to as the period of *reheating*.

It is fair to say that the nature of reheating is not well understood at the moment. One reason is that it is model dependent, with its features varying according to the couplings that connect the inflaton field to the Standard Model (or its extension). Another reason is that, even for known couplings, reheating represents a complicated process, given that the redistribution of the inflating energy density into an equipartitioned plasma of light particles requires multiple hard and soft interactions.

In the present paper, our goal is to address the physics of the reheating period in a somewhat model-independent way, by describing the inflaton-plasma interaction through an effective coupling of a low-energy description, and varying it in a broad range [6]. We treat the system as being composed of two subsystems: an inflaton field (φ), which interacts weakly with a strongly self-interacting radiation plasma, the latter carrying a seed temperature (T). The coupling between φ and the plasma is parameterized by the function $\Upsilon = \Upsilon(\varphi, T)$, which we refer to as the *inflaton equilibration rate*. Despite its simplicity, this system displays rich physics, manifested by the spectrum of its density perturbations. However, the general features of the dynamics can be described by a transparent set of equations, even if the nature of the solution depends on the functional forms of the inflaton potential and of Υ .

Though our fundamental interest concerns the reheating period, the physical system just outlined coincides with what has been studied for the model of *warm inflation* [7, 8]. The investigation of the corresponding density perturbations has a long history [9–12], and insights from complementary viewpoints [13–15]. In the past years, apart from model building, there have been new looks at the basic equations and their solutions [16–22], sometimes finding results that do not agree with previous estimates. Therefore, it appears worthwhile to test our reheating framework in the warm inflation context.

In fact, it turned out that our setup goes beyond the approximations often adopted for warm inflation in several respects. Denoting by k a comoving momentum, and by a the cosmological scale factor, the key ingredients of our study are:

- We determine the thermal noise autocorrelator so that it interpolates smoothly between the “classical” ($k/a \ll T$) and the “quantum” ($k/a \gg T$) domains, and is free from double counting (cf. sec. 3). In the same spirit, we impose quantum-mechanical initial conditions, so that they determine the solution if noise and dissipation are absent, and otherwise get gradually damped (cf. sec. 2.3).
- We invoke no slow-roll approximation, neither for the background evolution, nor for perturbations. In other words, our equations incorporate the decoupling of the inflaton field, when its energy density is below that of radiation, and the presence of acoustic oscillations, when a plasma mode is inside the Hubble horizon.
- We invoke no gauge fixing, neither for inflaton ($\delta\varphi$), nor plasma ($\delta T, \delta v$), nor metric (h_0, h_D, h, ϑ) perturbations, but rather solve a closed set of equations for three gauge-

invariant curvature perturbations (\mathcal{R}_φ , \mathcal{R}_v , \mathcal{R}_T). As a nice check of our numerics, the values of \mathcal{R}_φ , \mathcal{R}_v and \mathcal{R}_T coincide while a mode is outside of the Hubble horizon.

- We make no assumption about whether the inflaton field has equilibrated, but rather let our equations drive φ dynamically towards equilibrium (via dissipation and fluctuations). It is assumed, however, that the plasma with which φ interacts, is in local kinetic and helicity equilibrium (for recent discussions about these non-trivial assumptions, see refs. [15, 22]). Our setup allows for the self-interactions of the plasma to be strong; strongly interacting plasmas might open interesting avenues [23].
- We treat $Q \equiv \Upsilon/(3H)$ as a time-dependent variable, rather than fixing it to a constant while perturbations evolve (here $H \equiv \dot{a}/a$ is the Hubble rate). The functional form of Υ is determined by the underlying microscopic theory, and by the background evolution of the inflaton field and the temperature.

For these reasons, it is not guaranteed *a priori* whether our results agree exactly with the warm inflation ones. It is also not easy to anticipate the source of the differences, given that there are many points. We stress, however, that the differences are not associated with numerical issues or model dependence, but rather with the model-independent foundations of non-equilibrium quantum statistical physics in an expanding background.

Our presentation is organized as follows. The basic equations, initial conditions, and approximations valid in certain limits, are reviewed in sec. 2. Then we turn to the main theoretical ingredient of this work, the determination of the noise autocorrelator, in sec. 3. The methods that we have adopted for the numerical solution of the equations from sec. 2 are discussed in sec. 4, with illustrative benchmarks subsequently shown in sec. 5. A broad range of friction coefficients, interpolating between thermal and vacuum-like ones, are scanned in sec. 6, allowing us to compare with literature and scrutinize the universality of freeze-out predictions. The second application can be found in sec. 7, investigating a Standard Model embedded warm inflation scenario. Conclusions and an outlook are offered in sec. 8.

2. Evolution equations and initial conditions for perturbations

2.1. General set of gauge-invariant equations

A prototypical classical evolution equation for a real scalar field, φ , interacting with a thermal plasma, is offered by the Langevin equation,

$$\varphi^{;\mu}_{;\mu} - \Upsilon u^\mu \varphi_{,\mu} - V_{,\varphi} + \varrho = 0. \quad (2.1)$$

Here $(\dots)_{;\mu}$ is a covariant derivative; $(\dots)_{,\mu}$ is a normal derivative; u^μ is the plasma four-velocity; Υ is a friction coefficient, transporting energy from φ to the plasma; V is the scalar

field self-interaction potential, with $V_{,\varphi} \equiv \partial_{\varphi} V$; ϱ is a stochastic noise term, representing the energy that φ gains from plasma scatterings; and we assume the metric signature $(-+++)$.

Equation (2.1) should be viewed as a supplement to the conservation equations $T_{\mu\nu}{}^{;\mu} = 0$ that dictate the dynamics of the plasma. Similarly to the “constitutive relations” by which we express $T_{\mu\nu}$ in terms of thermodynamic potentials and the flow velocity, eq. (2.1) represents the leading terms of a derivative expansion, describing the low-energy dynamics of long-range degrees of freedom of φ . From a quantum-mechanical point of view, a non-trivial feature is that time reversal is not a symmetry. For $\Upsilon > 0$, dissipation and fluctuations drive the low-energy modes of φ towards the equilibrium state.

The properties of the noise, ϱ , are dictated by its autocorrelation function. The determination of the autocorrelation function is a key part of our investigation, and constitutes the contents of sec. 3.

We linearize eq. (2.1) around a background solution, $\varphi \equiv \bar{\varphi} + \delta\varphi$. We likewise linearize the Einstein equations, $\delta G_{\mu\nu} = 8\pi G \delta T_{\mu\nu}$, and energy-momentum conservation, $\delta T_{\mu\nu}{}^{;\mu} = 0$, where $G \equiv 1/m_{\text{pl}}^2$ is Newton’s constant, and $T_{\mu\nu}$ is the energy-momentum tensor describing the inflaton field φ and an ideal fluid [6, eq. (2.5)]. We account for scalar perturbations in the scalar field ($\delta\varphi$), temperature (δT), flow velocity (δv), and metric,

$$g_{\mu\nu} \equiv a^2 \begin{pmatrix} -1 - 2h_0 & \partial_i h \\ \partial_i h & (1 - 2h_{\text{D}})\delta_{ij} + 2(\partial_i \partial_j - \delta_{ij} \frac{\nabla^2}{3})\vartheta \end{pmatrix}. \quad (2.2)$$

In eq. (2.2), four scalar perturbations have been included (h_0 , h_{D} , h , ϑ). Through a linear transformation, the resulting set of evolution equations can be reduced to a 3×3 system (cf. eqs. (2.13)–(2.15) below), for the gauge-invariant variables

$$\mathcal{R}_{\varphi} \equiv -\left(h_{\text{D}} + \frac{\nabla^2 \vartheta}{3}\right) - H \frac{\delta\varphi}{\dot{\bar{\varphi}}}, \quad (2.3)$$

$$\mathcal{R}_v \equiv -\left(h_{\text{D}} + \frac{\nabla^2 \vartheta}{3}\right) + aH(h - \delta v), \quad (2.4)$$

$$\mathcal{R}_T \equiv -\left(h_{\text{D}} + \frac{\nabla^2 \vartheta}{3}\right) - H \frac{\delta T}{\dot{T}}. \quad (2.5)$$

These variables are referred to as *curvature perturbations*. The noise ϱ in eq. (2.1) is treated as being of the same order as $\delta\varphi$, δv and δT .

We can represent the perturbations and the noise as Fourier modes in spatial directions. There is however the delicate point that we want to *match* our solution to quantum-mechanical initial conditions. We then need a formalism which permits to incorporate both quantum-mechanical and statistical expectation values. A way to do this is to represent all linear perturbations in the language of a *mode expansion*,

$$\mathcal{R}_{\varphi} \equiv \int \frac{d^3\mathbf{k}}{\sqrt{(2\pi)^3}} \left[w_{\mathbf{k}} \mathcal{R}_{\varphi k}(t) e^{i\mathbf{k}\cdot\mathbf{x}} + w_{\mathbf{k}}^{\dagger} \mathcal{R}_{\varphi k}^*(t) e^{-i\mathbf{k}\cdot\mathbf{x}} \right], \quad (2.6)$$

where the annihilation and creation operators satisfy $[w_{\mathbf{k}}, w_{\mathbf{l}}^\dagger] \equiv \delta^{(3)}(\mathbf{k} - \mathbf{l})$. In the text-book interaction picture, the mode expansion is written for free fields, and the mode functions are solved from the corresponding classical field equations. In our situation, \mathcal{R}_φ interacts with the plasma degrees of freedom. To include this physics, we adopt a description in which the plasma interactions promote the mode functions, $\mathcal{R}_{\varphi k}$, to stochastic variables.

We can now define the quantum-mechanical and stochastic expectation values. For the quantum side, the observable of our interest reads

$$\langle 0 | \mathcal{R}_\varphi^2(t, \mathbf{x}) | 0 \rangle = \int_{-\infty}^{+\infty} d \ln k \frac{k^3}{2\pi^2} |\mathcal{R}_{\varphi k}(t)|^2, \quad (2.7)$$

where $|0\rangle$ refers to the distant-past (Bunch-Davies) vacuum, $w_{\mathbf{k}}|0\rangle = 0$, from which we assume the initial conditions to be sampled. The observed curvature power spectrum involves in addition an average over the possible stochastic realizations of the mode functions,

$$\langle \mathcal{P}_{\mathcal{R}_\varphi}(t, k) \rangle \equiv \frac{k^3}{2\pi^2} \langle |\mathcal{R}_{\varphi k}(t)|^2 \rangle. \quad (2.8)$$

Given that our equations are linear, we are free to rescale variables, without changing the form of the equations. It is convenient to write the power spectrum of eq. (2.8) directly as the absolute value squared of one of our dynamical variables,

$$\langle \mathcal{P}_{\mathcal{R}_\varphi}(t, k) \rangle \stackrel{(2.8)}{\underset{(2.10)}{=}} \langle |\mathcal{R}_k(t)|^2 \rangle. \quad (2.9)$$

To this aim, we define

$$\mathcal{R}_k \stackrel{(2.8)}{\underset{(2.9)}{=}} \frac{k^{3/2}}{\sqrt{2\pi^2}} \mathcal{R}_{\varphi k}, \quad (2.10)$$

$$\mathcal{S}_v \equiv \frac{k^{3/2}}{\sqrt{2\pi^2}} (\bar{e} + \bar{p})(\mathcal{R}_{vk} - \mathcal{R}_{\varphi k}), \quad (2.11)$$

$$\mathcal{S}_T \equiv \frac{k^{3/2}}{\sqrt{2\pi^2}} \bar{e}_{,T} \dot{T} (\mathcal{R}_{Tk} - \mathcal{R}_{\varphi k}), \quad (2.12)$$

where $f_{,x} \equiv \partial_x f$, and dots denote physical time derivatives (\bar{e} and \bar{p} are defined below eq. (2.16)). The variables \mathcal{S}_v and \mathcal{S}_T are called *isocurvature perturbations*, because the first (“curvature”) term from eqs. (2.3)–(2.5) drops out in the differences. The equations governing

the evolutions of these perturbations can be found in eqs. (3.42)–(3.44) of ref. [6],

$$\begin{aligned}\ddot{\mathcal{R}}_k &= -\frac{\varrho_k H}{\dot{\bar{\varphi}}} - \dot{\mathcal{R}}_k [\Upsilon + 2\mathcal{F} + 3H] - \mathcal{R}_k \left[\frac{k^2}{a^2} \right] \\ &\quad + \mathcal{S}_v \left[\frac{4\pi G(\Upsilon + 2\mathcal{F})}{H} \right] - \mathcal{S}_T \left[\frac{4\pi G}{H} \left(1 - \frac{\bar{p}_{,T}}{\bar{e}_{,T}} \right) + \frac{V_{,\varphi T} + \Upsilon_{,T} \dot{\bar{\varphi}}}{\dot{\bar{\varphi}} \bar{e}_{,T}} \right],\end{aligned}\quad (2.13)$$

$$\dot{\mathcal{S}}_v = -\dot{\mathcal{R}}_k [\bar{e} + \bar{p}] - \mathcal{S}_v \left[3H + \frac{4\pi G \dot{\bar{\varphi}}^2}{H} \right] + \mathcal{S}_T \left[\frac{\bar{p}_{,T}}{\bar{e}_{,T}} \right], \quad (2.14)$$

$$\begin{aligned}\dot{\mathcal{S}}_T &= \varrho_k \dot{\bar{\varphi}} H + \dot{\mathcal{R}}_k \left[\Upsilon \dot{\bar{\varphi}}^2 + \frac{8\pi G \bar{e}(\bar{e} + \bar{p})}{H} \right] - \mathcal{R}_k \left[(\bar{e} + \bar{p}) \frac{k^2}{a^2} \right] \\ &\quad - \mathcal{S}_v \left[\frac{k^2}{a^2} + \frac{4\pi G}{H} \left(\Upsilon \dot{\bar{\varphi}}^2 + \frac{8\pi G \bar{e}(\bar{e} + \bar{p})}{H} \right) \right] \\ &\quad + \mathcal{S}_T \left[\frac{\dot{H} - 4\pi G(\bar{e} + \bar{p})}{H} - 3H \left(1 + \frac{\bar{p}_{,T}}{\bar{e}_{,T}} \right) + \frac{(V_{,\varphi T} + \Upsilon_{,T} \dot{\bar{\varphi}}) \dot{\bar{\varphi}}}{\bar{e}_{,T}} \right],\end{aligned}\quad (2.15)$$

where the coefficient \mathcal{F} is defined as

$$\mathcal{F} \equiv \frac{H}{\dot{\bar{\varphi}}} \left(\frac{\dot{\bar{\varphi}}}{H} \right)' = \frac{\ddot{\bar{\varphi}}}{\dot{\bar{\varphi}}} - \frac{\dot{H}}{H}, \quad (2.16)$$

and $\bar{e} \equiv e_r + V$ and $\bar{p} \equiv p_r - V$ include only the non-derivative parts of the background energy density and pressure (the derivatives $\dot{\bar{\varphi}}^2$ are displayed separately). By e_r and p_r we denote the energy density and pressure of the plasma (“radiation”).

For the background evolution, we assume that thermal corrections to the scalar field potential are negligible, $V_{,T} \approx 0$.¹ Then the evolution equations read

$$\ddot{\bar{\varphi}} + (\Upsilon + 3H) \dot{\bar{\varphi}} + V_{,\varphi}(\bar{\varphi}) = 0, \quad (2.17)$$

$$\dot{e}_r + 3H(e_r + p_r) = \Upsilon \dot{\bar{\varphi}}^2, \quad (2.18)$$

$$\sqrt{\frac{8\pi}{3}} \frac{\sqrt{\frac{1}{2} \dot{\bar{\varphi}}^2 + e_r + V}}{m_{\text{pl}}} = H. \quad (2.19)$$

At late times, φ starts oscillating if the potential has positive curvature, and then the dynamics can be smoothly matched onto that of an averaged energy density, e_φ ; and finally, once $e_\varphi \ll e_r$, we can drop e_φ from the evolution equations. These transitions are important for quantitatively matching our solution to a reheated Standard Model plasma (cf. eq. (5.2)).

¹If this is not the case, warm inflation model building becomes challenging [13], however the background evolution equations themselves are not much more complicated (cf., e.g., eqs. (4.23)–(4.25) of ref. [6]).

Through eqs. (2.13)–(2.15), the problem has taken a purely classical appearance. Quantum mechanics lies in the initial conditions of the mode functions, and we return to them in sec. 2.3. Of course, it should be stressed that the corresponding solution does not represent an *exact* answer to the full quantum-statistical problem. Rather, it is an approximate answer, which has the correct quantum-mechanical limit when the plasma-dependent quantities have not yet played a role, as well as the correct classical limit when the system has equilibrated and all memory about initial conditions has been lost. At intermediate times, the solution smoothly interpolates between these limits. By tuning the noise, as will be described in sec. 3, we can however ensure that the solution is correct also deep inside the Hubble horizon, when both quantum and statistical fluctuations are present. Given that the solution exits the Hubble horizon exponentially fast, and freezes out almost immediately after having done so, we expect the third regime to guarantee that our solution represents a phenomenologically reasonable approximation to the full power spectrum.

2.2. Scale hierarchies and simplifications for the weak regime

The coefficients that appear in eqs. (2.13)–(2.15) vary rapidly with time, as dictated by the background solution. It may not be obvious at first sight which of them are the most important ones. However, the system does develop scale hierarchies during its evolution, implying that some terms matter more than others. Here we recall some of the key notions.

- (i) It is important to know the relations between the Hubble rate, H , the friction coefficient, Υ , and the temperature, T . The first two are themselves functions of $\bar{\varphi}$ and T . The relations between the three are time-dependent, and model-dependent. If $T, \Upsilon \gg H$, we say that we find ourselves in the *strong regime* (of warm inflation). Then the plasma influences both the background evolution, and first-order perturbations. If, instead, $\Upsilon \ll H \ll T$, we talk about a *weak regime*. In this case, thermal fluctuations may be important (cf. the discussion below eq. (3.31)), but Υ does not influence much the background evolution. Finally, if $T, \Upsilon \ll H$, a thermal plasma could still be present (provided that its internal equilibration rate satisfies $\Gamma \gg H$, which requires strong self-interactions), but it does not influence inflationary predictions.
- (ii) The coefficient that evolves most rapidly is the physical momentum, k/a . At early time, $k/a \gg H$, and the modes are inside the Hubble horizon. At intermediate times, $k/a \ll H$, and the modes are outside of the Hubble horizon. Then the modes are “frozen”, i.e. $\dot{\mathcal{R}}_k \approx 0$. At late times, the modes re-enter inside the Hubble horizon, $k/a \gg H$, and the system starts to undergo acoustic oscillations.
- (iii) In the course of time, the degree of freedom that carries the background energy density changes. In the standard picture, V is the dominant component at early times; $\dot{\bar{\varphi}}^2$ and

V are of similar magnitudes when inflation ends, and may remain the most important component for a while; ultimately, the plasma energy density takes over, and radiation-dominated expansion begins. We may expect that perturbations reflect this change. Notably, in the weak regime, even if \mathcal{S}_v and \mathcal{S}_T show a non-trivial evolution, they do not much affect the dynamics of \mathcal{R}_k ; and *vice versa*, at late times, after Hubble horizon re-entry, \mathcal{R}_k evolves, but this dynamics decouples from those of \mathcal{R}_{vk} and \mathcal{R}_{Tk} [6].

Making use of these scale hierarchies and restricting ourselves to a specific epoch, we can sometimes simplify the evolution equations. Let t_{out} denote a time at which a given mode is well outside of the Hubble horizon. Until this moment, and if φ dominates both the potential and kinetic energy, we expect the dynamics to be governed by the first line of eq. (2.13), *viz.*

$$\ddot{\mathcal{R}}_k + (\Upsilon + 2\mathcal{F} + 3H) \dot{\mathcal{R}}_k + \frac{k^2}{a^2} \mathcal{R}_k \stackrel[t \leq t_{\text{out}}]{e_r \ll \dot{\varphi}^2} \approx -\frac{\varrho_k H}{\dot{\varphi}}. \quad (2.20)$$

This truncation is gauge invariant, with the non-trivial information about going over to gauge-invariant variables contained in the coefficient \mathcal{F} from eq. (2.16). In terms of the nomenclature from point (i), we expect eq. (2.20) to be valid in the weak regime. It gets simplified further if we invoke one of the hierarchies mentioned under (ii). In sec. 5, we will compare the solution obtained from eq. (2.20) with the full solution resulting from eqs. (2.13)–(2.15), confirming that the difference becomes large in the strong regime (cf. fig. 3 on p. 20).

2.3. Classical representation of the quantum-mechanical initial state

With the help of eqs. (2.3), (2.6), (2.10), and (2.20), we can deduce the initial conditions for the mode function \mathcal{R}_k . Let us denote by $t_1 \ll t_{\text{out}}$ a time at which the mode considered is well inside the Hubble horizon but non-thermal, with $k/a_1 \gg T_1, \Upsilon_1 + 2\mathcal{F}_1 + 3H_1$, where we denote $f_1 \equiv f(t_1)$. Anticipating that the noise becomes exponentially suppressed in this regime, cf. eq. (3.30), eq. (2.20) is dominated by the two terms from its homogeneous part, rendering it the harmonic oscillator equation of motion,

$$\ddot{\mathcal{R}}_k + \frac{k^2}{a^2} \mathcal{R}_k \stackrel[t \leq t_1]{\approx} 0. \quad (2.21)$$

This has known trigonometric solutions. Choosing the *forward-propagating* one, as is appropriate for the mode expansion in eq. (2.6), we can express the first initial condition as

$$\dot{\mathcal{R}}_k(t_1) \approx -i \frac{k}{a_1} \mathcal{R}_k(t_1). \quad (2.22)$$

Let us stress that eq. (2.22) requires that $\mathcal{R}_k \in \mathbb{C}$.

The second initial condition originates from the fact that deep inside the Hubble horizon, $\delta\varphi$ in eq. (2.3) should be a local canonically normalized field, satisfying

$$[\delta\varphi(t_1, \mathbf{x}), \delta\dot{\varphi}(t_1, \mathbf{y})] = \frac{i\delta^{(3)}(\mathbf{x} - \mathbf{y})}{a_1^3}. \quad (2.23)$$

Here \mathbf{x} and \mathbf{y} are comoving rather than local Minkowskian coordinates, which produces the division by a_1^3 . From eq. (2.6), making use of the fact that the mode functions are symmetric in $\mathbf{k} \rightarrow -\mathbf{k}$, and suppressing the time argument t_1 , we find

$$\begin{aligned} [\mathcal{R}_\varphi(\mathbf{x}), \dot{\mathcal{R}}_\varphi(\mathbf{y})] &\stackrel{(2.6)}{\underset{\mathbf{k} \rightarrow -\mathbf{k}}{=}} \int \frac{d^3\mathbf{k}}{(2\pi)^3} \left\{ \mathcal{R}_{\varphi k} \overbrace{\dot{\mathcal{R}}_{\varphi k}^*}^{(2.22): i\frac{k}{a_1}\mathcal{R}_{\varphi k}^*} - \mathcal{R}_{\varphi k}^* \overbrace{\dot{\mathcal{R}}_{\varphi k}}^{-i\frac{k}{a_1}\mathcal{R}_{\varphi k}} \right\} e^{i\mathbf{k}\cdot(\mathbf{x}-\mathbf{y})} \\ &\stackrel{(2.22)}{\approx} \int \frac{d^3\mathbf{k}}{(2\pi)^3} \frac{2ik}{a_1} |\mathcal{R}_{\varphi k}|^2 e^{i\mathbf{k}\cdot(\mathbf{x}-\mathbf{y})} \stackrel{(2.3)}{\underset{(2.23)}{\approx}} \frac{H_1^2}{\dot{\varphi}_1^2} \frac{i\delta^{(3)}(\mathbf{x} - \mathbf{y})}{a_1^3} \\ &\Rightarrow |\mathcal{R}_{\varphi k}|^2 \approx \frac{H_1^2}{\dot{\varphi}_1^2} \frac{1}{2ka_1^2}. \end{aligned} \quad (2.24)$$

Including the rescaling by $k^{3/2}/\sqrt{2\pi^2}$ from eq. (2.10), and choosing a sign, this yields

$$\mathcal{R}_k(t_1) \stackrel{(2.24)}{\underset{(2.10)}{\approx}} \frac{H_1}{\dot{\varphi}_1} \frac{k}{2\pi a_1}. \quad (2.25)$$

Together with eq. (2.22), the initial conditions for \mathcal{R}_k have thereby been fixed. As we view the initial state as effectively non-thermal, with $k/a_1 \gg T_1$, we also set $\mathcal{S}_v(t_1) = \mathcal{S}_T(t_1) = 0$.

3. What an effective-theory perspective tells about the thermal noise

The next task is to determine the autocorrelator of the noise ϱ_k , appearing in eqs. (2.13), (2.15) and (2.20). We remark that the coefficient Υ can be determined independently of the noise, from linear response theory [24] or more general considerations [25], and we therefore assume that its value is known. Like in the classic Langevin equation, the noise is assumed to be white in time,

$$\langle \varrho_k(t) \varrho_k(t') \rangle = \Omega_k \delta(t - t'). \quad (3.1)$$

In the practical implementation we also treat it as Gaussian, even if this has formally no influence at the linear order to which we restrict ourselves (cf. eq. (4.9)).

We would like to fix the autocorrelator, Ω_k , so that the resulting power spectrum agrees with that predicted by quantum statistical physics in a certain limit. In practice, we consider times early enough so that $e_r \ll \dot{\varphi}^2$, allowing us to make use of the simplified eq. (2.20). We then proceed in four steps:

- (i) We choose coordinates and variables such that the problem looks Minkowskian. In essence, this means that we go to a local Minkowskian frame, but we implement this without making any approximation beyond eq. (2.20). We stress that the Minkowskian appearance concerns the first-order perturbations, whereas the background evolution is kept untouched (even if it were affected by Υ).
- (ii) In this frame, we determine the power spectrum with methods of *quantum* statistical physics. This means that the matching coefficients Υ and Ω_k of the classical description are omitted for a moment. The outcome of this thought experiment represents the correct answer, in the limit where the full system (φ + plasma) equilibrates. In general, only the plasma part is in equilibrium, with T defined as its local temperature.
- (iii) On the other side, we determine the power spectrum from the effective *classical* description, in the presence of Υ and Ω_k . Again we inspect how the results would look like in the idealized situation in which we could wait long enough that the full system equilibrates, even if in practice probably only the plasma does so.
- (iv) Equating the results of the thought experiments in steps (ii) and (iii), we can extract Ω_k (as mentioned above, the other matching coefficient Υ is assumed known).

Before going on with the concrete implementation of these steps, it is perhaps useful to answer the following question: if we are able to determine the full quantum-mechanical answer, from point (ii), why bother about the effective classical description, from point (iii)? The answer is that the classical framework has a broader range of applicability than the equilibrium quantum one, describing non-equilibrium situations as well, and indeed the very process of equilibration of φ .² This is essential for practical applications, as nothing guarantees that φ actually reaches the equilibrium state before the mode considered exits the Hubble horizon.

(i) choice of coordinates and variables. The goal of the first step is to eliminate \mathcal{F} and H from the friction term in eq. (2.20), so that only the thermal coefficient, Υ , remains. This can be achieved in three steps. First, we write $\mathcal{Q}_k \equiv -(\dot{\varphi}/H)\mathcal{R}_k$, which eliminates \mathcal{F} from the friction (but generates new terms, without derivatives acting on \mathcal{Q}_k). Second, we write $\hat{\mathcal{Q}}_k \equiv a\mathcal{Q}_k$. This eliminates $2H$ from the friction. Finally, we go to conformal time, with

$$dt = a d\tau, \quad (\dots)' \equiv \partial_\tau(\dots) = a \partial_t(\dots). \quad (3.2)$$

²Here we refer to the equilibration of the classical modes, with $k/a \ll T$. The equilibration rate is momentum dependent. At weak coupling, the quantum modes, with $k/a \geq T$, equilibrate faster than the classical ones, because their shorter wavelength permits for faster information transfer; as an example, for axion-like coupling, $\Upsilon(m \ll T \leq k/a) \sim \alpha_s^3 T^3 / f_a^2$, where α_s is the coupling of the non-Abelian theory [26].

This eliminates the remaining H . The end result takes the form given in eq. (4.8) of ref. [6],

$$\left(\partial_\tau^2 + \hat{\Upsilon} \partial_\tau + \overbrace{k^2 + \hat{\Upsilon} \hat{\mu} + \hat{m}^2}^{\equiv \hat{\epsilon}_k^2} \right) \hat{\mathcal{Q}}_k \stackrel{(2.20)}{\underset{[6, \text{eq. (4.8)}]}{\approx}} \hat{\varrho}_k, \quad (3.3)$$

$$\langle \hat{\varrho}_k(\tau) \hat{\varrho}_k(\tau') \rangle \stackrel{(3.1)}{\underset{(3.2)}{=}} \hat{\Omega}_k \delta(\tau - \tau'), \quad (3.4)$$

where we have defined “conformal” coefficients and functions as

$$\hat{\Upsilon} \equiv a \Upsilon, \quad \hat{\varrho}_k \equiv a^3 \varrho_k, \quad \hat{\Omega}_k \equiv a^5 \Omega_k, \quad (3.5)$$

$$\hat{\mu} \equiv -\frac{H}{\hat{\varphi}'} \left(\frac{\hat{\varphi}'}{H} \right)' \stackrel{\tau \leftrightarrow t}{\underset{(3.2), (2.16)}}{-a (\mathcal{F} + H)}, \quad (3.6)$$

$$\hat{m}^2 \equiv -\frac{H}{\hat{\varphi}'} \left(\frac{\hat{\varphi}'}{H} \right)'' \stackrel{\tau \leftrightarrow t}{\underset{(3.2), (2.16)}}{-a^2 (\partial_t + \mathcal{F} + 2H) (\mathcal{F} + H)}. \quad (3.7)$$

We have also denoted an energy-like variable as

$$\hat{\epsilon}_k^2 \equiv k^2 + \hat{\Upsilon} \hat{\mu} + \hat{m}^2 \equiv a^2 \epsilon_k^2, \quad (3.8)$$

$$\epsilon_k^2 = \frac{k^2}{a^2} - (\partial_t + \Upsilon + \mathcal{F} + 2H) (\mathcal{F} + H). \quad (3.9)$$

It may be wondered why we use the notation ϵ_k^2 in eq. (3.9), when it is not obvious if the quantity is positive. The reason can be understood by working out the second term of eq. (3.9) explicitly. By using a background evolution equation, we can write

$$\mathcal{F} \stackrel{(2.16)}{\underset{(2.17)}{=}} -\frac{V_{,\varphi}}{\hat{\varphi}} - \Upsilon - 3H - \frac{\dot{H}}{H}. \quad (3.10)$$

By taking a time derivative and using again eq. (2.17), we obtain $\dot{\mathcal{F}}$. Inserting into eq. (3.9) and combining terms, it can be shown that

$$\epsilon_k^2 \stackrel{(3.9)}{\underset{(2.17), (3.10)}}{\frac{k^2}{a^2}} + V_{,\varphi\varphi} + (\Upsilon + 2\mathcal{F} + 3H) \frac{\dot{H}}{H} + (\partial_t - H)(\Upsilon + 2H) + \frac{\ddot{H}}{H}. \quad (3.11)$$

From here we see that if we keep a and Υ constant, we get

$$\epsilon_k^2 \stackrel{(3.11)}{\underset{a, \Upsilon \rightarrow \text{const}}{\rightarrow}} \frac{k^2}{a^2} + V_{,\varphi\varphi}. \quad (3.12)$$

This is the normal Minkowskian definition of the energy squared, with the mass squared given by the curvature of a potential. On the other hand, during the slow-roll period, when $\mathcal{F} \ll H$ and $\dot{H} \ll H^2$, the would-be energy squared reads

$$\epsilon_k^2 \stackrel{(3.11)}{\underset{\dot{\Upsilon} \ll H\Upsilon, \dot{H} \ll H^2, \mathcal{F} \ll H}{\approx}} \frac{k^2}{a^2} - H (\Upsilon + 2H). \quad (3.13)$$

This becomes negative as k/a decreases. The definition of an “instantaneous” quantum-mechanical Hilbert space and statistical physics, required for our matching computation, is guaranteed to be sensible only when ϵ_k^2 is positive. However, the results have an analytic continuation also outside of this domain (see below) and, in any case, \mathcal{R}_k is observed to freeze out once a mode exits the Hubble horizon and $\epsilon_k^2 < 0$.

(ii) quantum-statistical equilibrium power spectrum. We now consider the system from eq. (3.3). After omitting the classical matching coefficients from the equations governing the perturbations (the background evolution is kept fixed), the mode equations satisfy

$$\hat{\mathcal{Q}}_k'' + \hat{\epsilon}_k^2 \hat{\mathcal{Q}}_k \underset{\hat{\Gamma}, \hat{\Omega}_k \rightarrow 0}{\overset{(3.3)}{\approx}} 0. \quad (3.14)$$

The corresponding field operator is like in eq. (2.6), after recalling the rescaling from eq. (2.10),

$$\hat{\mathcal{Q}}_\varphi \equiv \int \frac{d^3\mathbf{k}}{\sqrt{(2\pi)^3}} \left[w_{\mathbf{k}} \hat{\mathcal{Q}}_{\varphi k}(t) e^{i\mathbf{k}\cdot\mathbf{x}} + w_{\mathbf{k}}^\dagger \hat{\mathcal{Q}}_{\varphi k}^*(t) e^{-i\mathbf{k}\cdot\mathbf{x}} \right], \quad \hat{\mathcal{Q}}_k \equiv \frac{k^{3/2}}{\sqrt{2\pi^2}} \hat{\mathcal{Q}}_{\varphi k}. \quad (3.15)$$

Forward-propagating mode functions are defined like in eq. (2.22), $\hat{\mathcal{Q}}_k' = -i\hat{\epsilon}_k \hat{\mathcal{Q}}_k$, and a canonical commutator like in eq. (2.23), $[\hat{\mathcal{Q}}_\varphi(\mathbf{x}), \hat{\mathcal{Q}}_\varphi'(\mathbf{y})] = i\delta^{(3)}(\mathbf{x} - \mathbf{y})$. The result is analogous to eq. (2.24), except that we now do *not* assume k asymptotically large, so that k is replaced by $\hat{\epsilon}_k$, leading to $|\hat{\mathcal{Q}}_{\varphi k}|^2 = 1/(2\hat{\epsilon}_k)$. Subsequently, the vacuum power spectrum is

$$\langle \tilde{0} | \hat{\mathcal{Q}}_\varphi^2(\mathbf{x}) | \tilde{0} \rangle = \int \frac{d^3\mathbf{k}}{(2\pi)^3} |\hat{\mathcal{Q}}_{\varphi k}|^2 = \int \frac{d^3\mathbf{k}}{(2\pi)^3} \frac{1}{2\hat{\epsilon}_k}, \quad (3.16)$$

where $|\tilde{0}\rangle$ denotes an instantaneous vacuum in the local Minkowskian frame. These relations are sensible only when $\hat{\epsilon}_k > 0$.

Next, we introduce a finite temperature. The underlying assumption, made for the purpose of matching, is that φ has time to equilibrate to the instantaneous temperature T , defined by the plasma component. The equilibration process does not need to be completed in practice, because our subsequent classical description also holds when φ is out of equilibrium. However, the presence of a plasma drives the system *towards* equilibrium.

When we go from vacuum expectation values to quantum statistical physics within free field theory, the mode functions do *not* change, but the ensemble is different. Considering an excited state with $n_{\mathbf{q}} \geq 0$ quanta of momentum \mathbf{q} , non-vanishing matrix elements contributing to a trace are

$$\langle \dots; n_{\mathbf{q}}; \dots | w_{\mathbf{k}} w_{\mathbf{q}}^\dagger | \dots; n_{\mathbf{q}}; \dots \rangle = \delta^{(3)}(\mathbf{k} - \mathbf{q}) (1 + n_{\mathbf{q}}), \quad (3.17)$$

$$\langle \dots; n_{\mathbf{q}}; \dots | w_{\mathbf{k}}^\dagger w_{\mathbf{q}} | \dots; n_{\mathbf{q}}; \dots \rangle = \delta^{(3)}(\mathbf{k} - \mathbf{q}) n_{\mathbf{q}}. \quad (3.18)$$

The expectation value that includes simultaneously both quantum and statistical effects is

$$\langle \hat{\mathcal{Q}}_\varphi^2(\mathbf{x}) \rangle_T \equiv \frac{\text{tr} [e^{-\hat{H}/T} \hat{\mathcal{Q}}_\varphi^2(\mathbf{x})]}{\text{tr} [e^{-\hat{H}/T}]}, \quad (3.19)$$

where \hat{H} is the Hamiltonian. Recalling our conformal units, the possible occupancies of the momentum mode \mathbf{q} contribute as

$$\frac{\sum_{n_{\mathbf{q}}=0}^{\infty} n_{\mathbf{q}} \exp(-\frac{\hat{\epsilon}_{\mathbf{q}} n_{\mathbf{q}}}{aT})}{\sum_{n_{\mathbf{q}}=0}^{\infty} \exp(-\frac{\hat{\epsilon}_{\mathbf{q}} n_{\mathbf{q}}}{aT})} = \frac{(-aT) \frac{d}{d\hat{\epsilon}_{\mathbf{q}}} \frac{1}{1 - \exp(-\frac{\hat{\epsilon}_{\mathbf{q}}}{aT})}}{\frac{1}{1 - \exp(-\frac{\hat{\epsilon}_{\mathbf{q}}}{aT})}} = \frac{1}{\underbrace{\exp(\frac{\hat{\epsilon}_{\mathbf{q}}}{aT}) - 1}_{\equiv \hat{n}_{\text{B}}(\frac{\hat{\epsilon}_{\mathbf{q}}}{aT})}}. \quad (3.20)$$

All in all, this yields

$$\langle \hat{\mathcal{Q}}_\varphi^2(\mathbf{x}) \rangle_T \stackrel{(3.15)-(3.20)}{=} \int \frac{d^3\mathbf{k}}{(2\pi)^3} \frac{1}{2\hat{\epsilon}_k} \left[1 + 2\hat{n}_{\text{B}}\left(\frac{\hat{\epsilon}_k}{aT}\right) \right]. \quad (3.21)$$

The power spectrum, $|\hat{\mathcal{Q}}_k|^2$, is given by the integrand of eq. (3.21) after carrying out the (trivial) angular integrals in spherical coordinates, which yields the same volume element $k^3/(2\pi^2)$ as seen in eq. (3.15),

$$|\hat{\mathcal{Q}}_k|^2 \stackrel{(3.15)}{=} \stackrel{(3.21)}{=} \frac{k^3}{4\pi^2 \hat{\epsilon}_k} \left[1 + 2\hat{n}_{\text{B}}\left(\frac{\hat{\epsilon}_k}{aT}\right) \right]. \quad (3.22)$$

(iii) classical-statistical equilibrium power spectrum. Next, we return to eq. (3.3) and solve it (classically) in the presence of $\hat{\Upsilon}$ and ϱ_k . Furthermore, we again assume that equilibration to a temperature T happens faster than the variation of the parameter values $(\hat{\Upsilon}, \hat{\epsilon}_k)$. Under this assumption, we determine the classical approximation to $|\hat{\mathcal{Q}}_k|^2$.

Equation eq. (3.3) has a general homogeneous solution, and a special solution of the inhomogeneous equation. The homogeneous solution is identified with the quantum-mechanical initial conditions, which fix the two integration constants. To infer the thermal modifications, because of the assumed equilibration, we can wait long enough that the homogeneous solution has dissipated away. Then we only need to determine the special solution, and this can be done with the help of a retarded Green's function. Let us illustrate how this goes.

Inserting $\delta(\tau - \tau_1)$ as the right-hand side, the solution of eq. (3.3) is given by

$$G_k(\tau, \tau_1) \equiv \int \frac{d\omega}{2\pi} e^{-i\omega(\tau - \tau_1)} G_k(\omega), \quad G_k(\omega) \equiv \frac{1}{-\omega^2 + \hat{\Upsilon}(-i\omega) + \hat{\epsilon}_k^2}. \quad (3.23)$$

The poles lie at

$$\omega = -\frac{i\hat{\Upsilon}}{2} \pm X, \quad X \equiv \sqrt{\hat{\epsilon}_k^2 - \frac{\hat{\Upsilon}^2}{4}}. \quad (3.24)$$

For $\hat{\Upsilon} > 0$ and $\hat{\epsilon}_k^2 > 0$, so that $|\text{Im } X| < \hat{\Upsilon}/2$, the poles are in the lower half-plane. On the other hand, for $\tau - \tau_1 < 0$, we can close the ω -contour in eq. (3.23) in the upper half-plane, because the ω -integrand is exponentially suppressed there. As there are no poles in the upper half-plane, the integral vanishes, i.e. $G_k(\tau, \tau_1) = 0$ for $\tau < \tau_1$. Therefore, eq. (3.23) defines a *retarded* Green's function (i.e. it is non-zero only for $\tau > \tau_1$).

With the help of G_k from eq. (3.23), and assuming that $\hat{\Upsilon}$ and $\hat{\epsilon}_k^2$ are to a good approximation constant during the interval considered, a special solution of eq. (3.3) is given by

$$\hat{\mathcal{Q}}_k(\tau) \stackrel{(3.3)}{=} \int_{\tau_1} G_k(\tau, \tau_1) \hat{\varrho}_k(\tau_1) = \int_{\tau_1, \omega_1} e^{-i\omega_1(\tau - \tau_1)} G_k(\omega_1) \hat{\varrho}_k(\tau_1), \quad (3.25)$$

$$\int_{\tau_1} \equiv \int_{-\infty}^{+\infty} d\tau_1, \quad \int_{\omega_1} \equiv \int_{-\infty}^{+\infty} \frac{d\omega_1}{2\pi}. \quad (3.26)$$

Inserting

$$\hat{\mathcal{Q}}_k^*(\tau) = \int_{\tau_2, \omega_2} e^{i\omega_2(\tau - \tau_2)} G_k^*(\omega_2) \hat{\varrho}_k^*(\tau_2), \quad (3.27)$$

the power spectrum becomes

$$\begin{aligned} |\hat{\mathcal{Q}}_k(\tau)|^2 &\stackrel{(3.26)}{=} \int_{\tau_1, \tau_2, \omega_1, \omega_2} e^{i\omega_2(\tau - \tau_2) - i\omega_1(\tau - \tau_1)} G_k(\omega_1) G_k^*(\omega_2) \overbrace{\langle \hat{\varrho}_k(\tau_1) \hat{\varrho}_k^*(\tau_2) \rangle}^{(3.4) : \hat{\Omega}_k \delta(\tau_1 - \tau_2)} \\ &= \hat{\Omega}_k \int_{\tau_1, \omega_1, \omega_2} e^{i(\omega_2 - \omega_1)(\tau - \tau_1)} G_k(\omega_1) G_k^*(\omega_2) \\ &= \hat{\Omega}_k \int_{\omega_1} G_k(\omega_1) G_k^*(\omega_1) \\ &\stackrel{(3.23)}{=} \int_{-\infty}^{+\infty} \frac{d\omega_1}{2\pi} \frac{\hat{\Omega}_k}{(\omega_1 + \frac{i\hat{\Upsilon}}{2} + X)(\omega_1 + \frac{i\hat{\Upsilon}}{2} - X)(\omega_1 - \frac{i\hat{\Upsilon}}{2} + X)(\omega_1 - \frac{i\hat{\Upsilon}}{2} - X)} \\ &\stackrel{(3.24)}{=} \frac{\hat{\Omega}_k}{2X\hat{\Upsilon}} \left(\frac{1}{i\hat{\Upsilon} + 2X} + \frac{1}{-i\hat{\Upsilon} + 2X} \right) \stackrel{(3.24)}{=} \frac{\hat{\Omega}_k}{2\hat{\Upsilon}} \frac{1}{\hat{\epsilon}_k^2}. \end{aligned} \quad (3.28)$$

(iv) matching between quantum and classical descriptions. We compare eqs. (3.22) and (3.28), recalling that the temperature-independent first term of eq. (3.22) corresponds to the homogeneous solution, which was excluded from eq. (3.28). In other words, matching requires

$$\underbrace{\frac{k^3}{2\pi^2 \hat{\epsilon}_k} \hat{n}_B\left(\frac{\hat{\epsilon}_k}{aT}\right)}_{\text{from (3.22)}} \simeq \underbrace{\frac{\hat{\Omega}_k}{2\hat{\Upsilon}} \frac{1}{\hat{\epsilon}_k^2}}_{\text{from (3.28)}} \Rightarrow \hat{\Omega}_k \simeq 2\hat{\Upsilon} \hat{\epsilon}_k \hat{n}_B\left(\frac{\hat{\epsilon}_k}{aT}\right) \frac{k^3}{2\pi^2}. \quad (3.29)$$

Going back to physical units, via eqs. (3.5)–(3.9), then yields

$$\boxed{\Omega_k \stackrel{(3.29)}{\underset{(3.5)-(3.9)}{\simeq}} 2\Upsilon \epsilon_k n_{\text{B}}(\epsilon_k) \frac{(k/a)^3}{2\pi^2}}, \quad (3.30)$$

where the Bose distribution is defined as $n_{\text{B}}(x) \equiv 1/(e^{x/T} - 1)$, and ϵ_k is from eq. (3.9).

Let us elaborate on how eq. (3.30) should be interpreted in different regimes:

- $\epsilon_k \geq T$. In this domain, the noise autocorrelator from eq. (3.30) is exponentially suppressed. Then the evolution reflects quantum-mechanical initial conditions.
- $0 < \epsilon_k \ll T$. Because of the negative terms in eq. (3.13), ϵ_k decreases as the mode considered is close to exiting the Hubble horizon. In this domain, we can approximate

$$n_{\text{B}}(x) \stackrel{|x| \ll T}{\approx} \frac{T}{x} \Rightarrow \Omega_k \stackrel{(3.30)}{\underset{\epsilon_k \ll T}{\approx}} 2\Upsilon T \frac{(k/a)^3}{2\pi^2}. \quad (3.31)$$

This corresponds to the textbook fluctuation-dissipation relation (modified by our convention of including the phase-space volume element in Ω_k). According to eq. (3.13), eq. (3.31) is a good approximation to eq. (3.30) in the domain $k^2/a^2 \ll (\Upsilon + 2H)H + T^2$. Thermal fluctuations have a large effect before freeze-out if $T^2 \gg (\Upsilon + 2H)H$.

- $\epsilon_k^2 \leq 0$. When ϵ_k^2 becomes negative, our derivation is not physically sensible. That said, eq. (3.31) is independent of ϵ_k^2 , and can be employed as an extrapolation into this domain. Mathematically speaking, it represents a good approximation to the analytic continuation of eq. (3.30) as long as $|\epsilon_k| < 2\pi T$, before n_{B} develops additional poles along the imaginary axis. Physically speaking, the rapidly decreasing $(k/a)^3$ guarantees that the noise only plays a minor role outside of the Hubble horizon. Therefore, we employ eq. (3.31) in the domain $\epsilon_k^2 < 0$.

4. Numerical method for the stochastic evolution

The noise autocorrelator in eq. (3.30) is a strongly varying function of time, but it does not depend on the dynamical variable that it affects, \mathcal{R}_k . Therefore, the stochastic evolution equations can be discretized by making use of the standard Itô or Stratonovich schemes. For us the Itô scheme turned out to be sufficient, so we describe its practical implementation, as well as the simplifications that are possible if only the power spectrum is required (in contrast to the full probability distribution). The same procedure works both for the full dynamics from eqs. (2.13)–(2.15), and for the simplified evolution from eq. (2.20).

Given that the coefficients vary rapidly with time, it is important to choose a dynamically changing time step. Let us assemble our variables into a vector,

$$\mathcal{V} \equiv (\mathcal{R}_k \dot{\mathcal{R}}_k \mathcal{S}_v \mathcal{S}_T)^\text{T}, \quad (4.1)$$

where $(\dots)^T$ denotes a transpose. Regularizing the poles appearing in eq. (2.20) as in ref. [6],

$$\mathcal{F} \xrightarrow{(2.16)} \frac{\ddot{\bar{\varphi}}}{\dot{\bar{\varphi}} + i\delta} - \frac{\dot{H}}{H}, \quad -\frac{\varrho_k H}{\dot{\bar{\varphi}}} \rightarrow -\frac{\varrho_k H}{\dot{\bar{\varphi}} + i\delta}, \quad (4.2)$$

our continuum equation has the form

$$\dot{\mathcal{V}} \stackrel{(2.20)}{\equiv} \stackrel{(4.1)}{\left(\overbrace{\begin{pmatrix} 0 & 1 & 0 & 0 \\ -\frac{k^2}{a^2} & -(\Upsilon + 2\mathcal{F} + 3H) & \dots \\ \vdots & \vdots & \ddots \end{pmatrix}}^{\equiv M} \right) \mathcal{V} + \mathcal{N}, \quad (4.3)$$

$$\langle \mathcal{N}_2(t) \mathcal{N}_2(t') \rangle \stackrel{(3.1)}{\equiv} \stackrel{(3.30), (4.2)}{\underbrace{2\Upsilon \epsilon_k n_B(\epsilon_k) \frac{(k/a)^3}{2\pi^2} \frac{H^2}{(\dot{\bar{\varphi}} + i\delta)^2}}_{\equiv W_{22}}} \delta(t - t'). \quad (4.4)$$

In eq. (4.3), we have shown explicitly only the parts originating from eq. (2.20), with the dots denoting the further terms from eqs. (2.13)–(2.15). The matrix M is called the drift term, \mathcal{N} the noise term, and W the noise autocorrelator.

A simple discretization of eq. (4.3) amounts to

$$\frac{\mathcal{V}_{i+1} - \mathcal{V}_i}{\epsilon_i} = M_i \mathcal{V}_i + \frac{\mathcal{N}_i}{\sqrt{\epsilon_i}}, \quad \langle \mathcal{N}_i^T \mathcal{N}_j \rangle = W_i \delta_{ij}, \quad (4.5)$$

where $f_i \equiv f(t_i)$ and $t_{i+1} - t_i \equiv \epsilon_i$. This yields the Itô evolution,

$$\mathcal{V}_{i+1} = (1 + \epsilon_i M_i) \mathcal{V}_i + \sqrt{\epsilon_i} \mathcal{N}_i. \quad (4.6)$$

A crucial question is how to choose ϵ_i , so that the evolution is stable and close to the correct continuum limit without an enormous computational cost. We base the criterion on the drift term, setting

$$\epsilon_i = \frac{\text{tol}}{\max\{|\lambda_i|\}}, \quad \text{tol} \ll 1.0, \quad (4.7)$$

where λ_i are the (complex) eigenvalues of M_i , and a sufficient tolerance is $\text{tol} \lesssim 10^{-3}$.

The matrix M in eq. (4.3) and the noise autocorrelator W in eq. (4.4) are functions of the background solution. Therefore, for a practical implementation, we first determine the background solution from eqs. (2.17)–(2.19). The solution is smooth, and can be stored in an array. With this information, eq. (4.6) is straightforward to evolve, with the (complex) Gaussian noise generated according to the variance given in eq. (4.5). In other words, if σ_i is

a Gaussian random variable, with variance $\langle \sigma_i^2 \rangle = 1$, then³

$$\mathcal{N}_{2i} \stackrel{(4.4)}{=} \stackrel{(4.5)}{-\sigma_i} \left[\sqrt{2\Upsilon \epsilon_k n_B(\epsilon_k)} \frac{(k/a)^{3/2}}{\sqrt{2\pi^2}} \frac{H}{\dot{\bar{\varphi}} + i\delta} \right]_{t=t_i}. \quad (4.8)$$

The function $\epsilon_k n_B(\epsilon_k)$ is extrapolated to the domain of non-positive arguments according to eq. (3.31). We remark that, when $\bar{\varphi}$ starts oscillating, the coefficient \mathcal{F} needs to be regularized according to eq. (4.2), and ϵ_k^2 from eq. (3.11) obtains an imaginary part. There is no principal problem with the variables becoming complex (the perturbations have been complexified by the initial conditions, cf. eq. (2.22)). Moreover, in our case the freeze-out dynamics takes place before $\bar{\varphi}$ starts oscillating, and the regularization plays no practical role.

If we are only interested in the power spectrum (cf. eq. (2.9)), the stochastic evolution can be greatly simplified. Taking the conjugate of eq. (4.6), multiplying with eq. (4.6), and noting that \mathcal{V}_i and \mathcal{N}_i are uncorrelated because \mathcal{V}_i is affected only by \mathcal{N}_{i-1} , we find

$$\langle \mathcal{V}_{i+1} \mathcal{V}_{i+1}^\dagger \rangle \stackrel{(4.6)}{=} (1 + \epsilon_i M_i) \langle \mathcal{V}_i \mathcal{V}_i^\dagger \rangle (1 + \epsilon_i M_i^\dagger) + \epsilon_i \langle \mathcal{N}_i \mathcal{N}_i^\dagger \rangle. \quad (4.9)$$

The initial conditions from eqs. (2.22) and (2.25) reside in a 2×2 subblock of $\langle \mathcal{V}_0 \mathcal{V}_0^\dagger \rangle$, and the stochastic noise makes a 2×2 subblock matrix out of $\langle \mathcal{N}_i \mathcal{N}_i^\dagger \rangle$, after inserting $\langle \sigma_i^2 \rangle = 1$. Thereby the evolution of the stochastic expectation values is deterministic. This approach was referred to as a *matrix formalism* in refs. [17, 18], who first demonstrated its effectiveness in the warm inflation context. Our scan results in figs. 5–7 are based on eq. (4.9).

5. Benchmarks and overall features

In this section we illustrate features of the solution of our evolution equations from sec. 4 with a few representative benchmarks. Subsequently, in secs. 6 and 7, we report our first physics applications, based on comprehensive scans of such solutions. We recall that, when $k \ll aH$, all curvature perturbations coincide; in that domain we streamline the notation by dropping the subscript from \mathcal{R}_φ or \mathcal{R}_k , so that we refer to the power spectrum as $\mathcal{P}_\mathcal{R}$.

For a transparent discussion, it is helpful to keep the parameters of the inflaton potential, the characteristics of the radiation plasma, and the initial conditions, fixed throughout the scans; they are chosen as explained in appendix A. The quantities varied are the friction coefficient, Υ , and the momentum mode considered, k . Let us anticipate that in phenomenological scans, it is necessary to vary the parameters of the inflaton potential as well, and indeed we will do this for our second application, in sec. 7.

³In practice, we take t/t_{ref} as the integration variable, where t_{ref} is defined in eq. (A.4). Then M and W get rescaled by $t_{\text{ref}} = H_{\text{ref}}^{-1}$. We note that \mathcal{N} in eq. (4.3) gets rescaled by H_{ref}^{-1} , so naively it looks like there is H_{ref}^{-2} in the autocorrelator, however we also have to write $H_{\text{ref}}^{-1} \delta(t - t') = \delta(t/t_{\text{ref}} - t'/t_{\text{ref}})$, whereby only one H_{ref}^{-1} is left over. In other words, \mathcal{N}_{2i} in eq. (4.8) is rescaled by $1/\sqrt{H_{\text{ref}}}$.

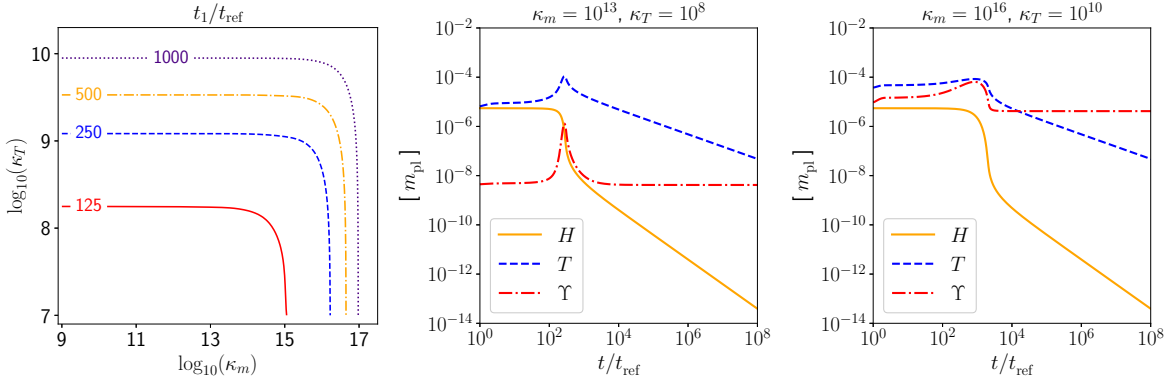


Figure 1: Left: keeping the inflaton potential (cf. eqs. (A.1), (A.2)) and the initial conditions fixed (cf. eqs. (A.3), (A.6)), the contours indicate the time t_1 (in units of t_{ref} from eq. (A.4)) at which the “pivot scale”, $k_*/a_0 = 0.05 \text{ Mpc}^{-1}$, reaches the value $k_*/(aH) = 10^2$, as a function of the parameters κ_m and κ_T determining the friction (cf. eq. (5.1)). The perturbations are initialized at this moment, cf. eqs. (2.22) and (2.25). Middle and right: the background solution from eqs. (2.17)–(2.19) for $\kappa_m = 10^{13}$, $\kappa_T = 10^8$ and $\kappa_m = 10^{16}$, $\kappa_T = 10^{10}$, respectively. The first choice corresponds to a weak regime, the second to a strong regime of warm inflation, in the sense defined under point (i) in sec. 2.2. The curvature perturbations corresponding to these solutions are shown in fig. 2.

For the friction coefficient, we employ a parametrization motivated by the structure originating from an axion-like coupling between the inflaton field and a non-Abelian plasma, with the latter assumed to be in kinetic and helicity equilibrium,

$$\Upsilon \equiv \frac{\kappa_T (\pi T)^3 + \kappa_m m^3}{(4\pi)^3 f_a^2}. \quad (5.1)$$

The parameters m and f_a are the same as in eq. (A.1). In a microscopic derivation, κ_T and κ_m depend on the coupling α_s of the non-Abelian theory, and on logarithms of T and m , and realistic values are of order $\kappa_T, \kappa_m \sim 1$ [24]. Moreover, a thorough study reveals a richer functional form than in eq. (5.1) [27]. However, values of order unity lead to very small thermal effects for CMB observables with the potential from eq. (A.1) [28]. In order to span trajectories with large thermal corrections, we scan the domains $\kappa_T \sim 10^{7.0 \dots 10.5}$ and $\kappa_m \sim 10^{9.0 \dots 17.5}$. The upper bounds yield solutions deep in the strong regime, which become increasingly costly to handle numerically, because the dynamics is dominated by fast acoustic oscillations of the radiation plasma (cf. fig. 2 on p. 19).

In order to consider physically commensurate values of k , we match the solution to a late universe. This means that we consider a time at which inflation has ended, φ has ceased to influence the background solution ($\Upsilon \gg H$), and the universe undergoes radiation-dominated expansion. As a convenient choice, we adopt the moment $T = T_e \equiv 10^{-12} m_{\text{pl}}$, which is reached at the time $t_e \approx 0.301 m_{\text{pl}} / (\sqrt{g_*} T_e^2)$, with g_* defined by eq. (A.5). By making use of Standard Model thermodynamics [29], we can estimate that the scale factor

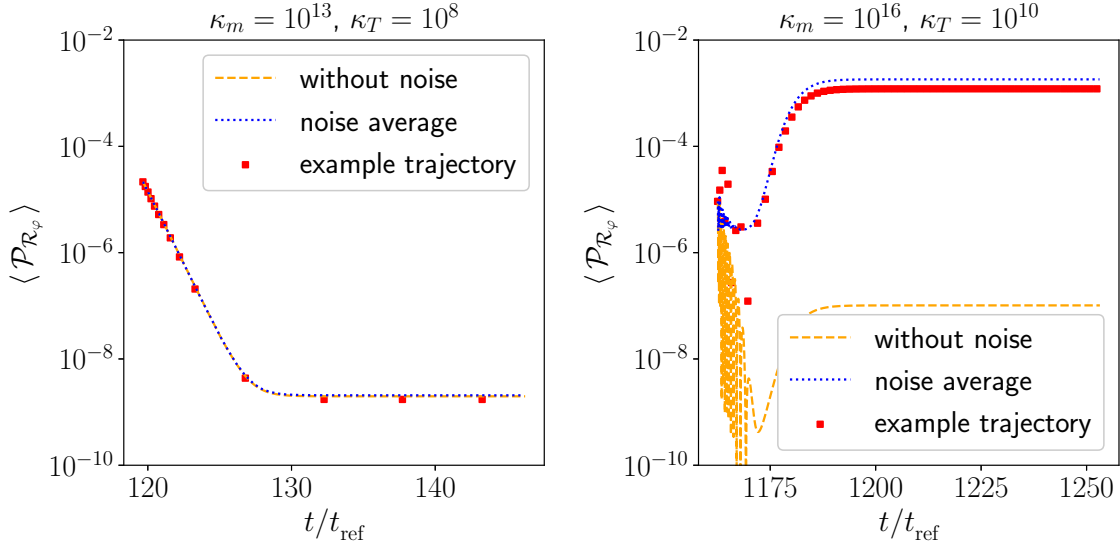


Figure 2: The curvature perturbations corresponding to the background solutions shown in fig. 1. The evolution was started at $k_*/(aH) = 10^2$. The dashed orange curve is a solution of eq. (4.9) but without noise, obtained by setting $\text{tol} = 10^{-3}$ in eq. (4.7). In the dotted blue curve, the noise average has been included. The red squares show an example trajectory from the stochastic eq. (4.6) (for better visibility, only a subset of points are shown). For the parameters at left, the noise has no visible effect. For the parameters at right, the noiseless solution undergoes acoustic oscillations while decaying. The noise compensates for the damping by generating new fluctuations. Around the time of the horizon exit, the curvature perturbations \mathcal{R}_v and \mathcal{R}_T drag \mathcal{R}_φ to a large common value.

increases by $a_0/a_e \approx e^{46.5}$ from the chosen T_e until today. The standard “pivot scale” for CMB observations today is $k_*/a_0 = 0.05 \text{ Mpc}^{-1}$. So, we are interested in modes which have $k_*/a_e = (k_*/a_0)(a_0/a_e) = 0.05 \text{ Mpc}^{-1} e^{46.5} \approx 4.10 \times 10^{-39} m_{\text{pl}}$. Having determined the time history of the background solution, we can backtrack from t_e until a time t_1 at which

$$\frac{k_*}{a_1 H_1} = \underbrace{\frac{k_*}{a_e m_{\text{pl}}}}_{4.10 \times 10^{-39}} \underbrace{\frac{a_e}{a_1}}_{e^{N_e - N_1}} \frac{m_{\text{pl}}}{H_1} \equiv 10^2. \quad (5.2)$$

This is the moment at which we start evolving the density perturbations (cf. sec. 2.3). The value of t_1 , in units of t_{ref} from eq. (A.4), is plotted in the plane (κ_m, κ_T) in fig. 1(left).

Numerical solutions of the background evolution for representative choices of κ_m and κ_T are shown in fig. 1(middle,right). The time evolutions of the corresponding curvature power spectra are illustrated in fig. 2. We show three variants: a solution for the averaged $\langle \mathcal{P}_{\mathcal{R}_\varphi} \rangle$ from eq. (4.9) but without noise; a solution of eq. (4.9) with noise included; and one trajectory from a solution of the full stochastic eq. (4.6). The probability distributions from a statistics of 10^3 trajectories obtained from eq. (4.6) are shown in fig. 3.

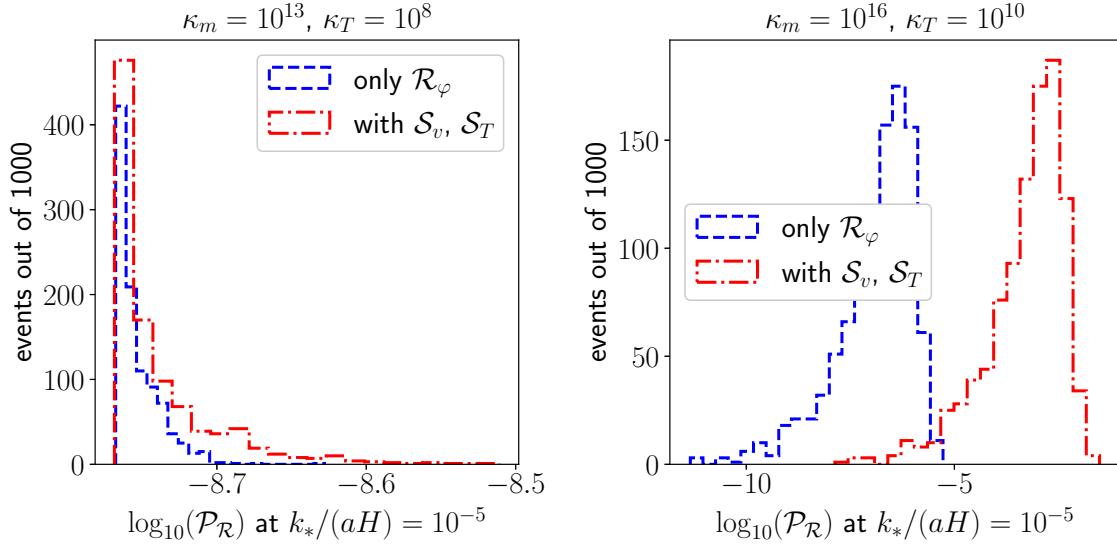


Figure 3: The probability distributions of the curvature power spectra for the two benchmarks from fig. 2, from the weak (left) and strong (right) regime (the individual bins are broader for a broader distribution, so the areas do not look the same). The skewed distribution on the right resembles the one found in ref. [18], where its shape and relation to $\log_{10}\langle\mathcal{P}_{\mathcal{R}}\rangle$ were also determined.

It is appropriate to remark that if $T \gg H$, then $k/(aT)$ is moderate at the initial time, $t = t_1$ (cf. eq. (5.2)), and the noise amplitude from eq. (4.8) is not exponentially suppressed. However, we find that the results stay the same also for earlier starting times, say $k_*/(a_1 H_1) = 10^3$, when the exponential suppression of the noise autocorrelator is clearly visible. The reason is that the initial noise only excites acoustic oscillations, which do not influence the value of the curvature perturbation around its freeze-out point.

To summarize the features observed in figs. 1, 2 and 3, the presence of $\Upsilon, \varrho \neq 0$ influences the dynamics of the system in many ways. The background solution is modified, which changes the way in which momenta redshift (cf. fig. 1(left)). On the side of perturbations, the original quantum fluctuations get dissipated, if $\Upsilon > H$ before they exit the Hubble horizon (cf. fig. 2). At the same time, new thermal fluctuations are generated, if $T > H$ during the same period (cf. fig. 2). An important point, visible from 2(right), is that the presence of \mathcal{R}_v and \mathcal{R}_T (through \mathcal{S}_v and \mathcal{S}_T , cf. eqs. (2.11) and (2.12)) has a large influence on \mathcal{R}_φ : \mathcal{S}_v and \mathcal{S}_T vanish outside of the Hubble horizon, and therefore \mathcal{R}_v and \mathcal{R}_T pull \mathcal{R}_φ up to their common value before the solution settles to a constant. Effectively, this means that \mathcal{R}_v and \mathcal{R}_T from eqs. (2.4) and (2.5) determine that final value of $\mathcal{P}_{\mathcal{R}}$. The probability distribution of $\log_{10} \mathcal{P}_{\mathcal{R}}$ is skewed (cf. fig. 3), as elaborated upon in ref. [18].

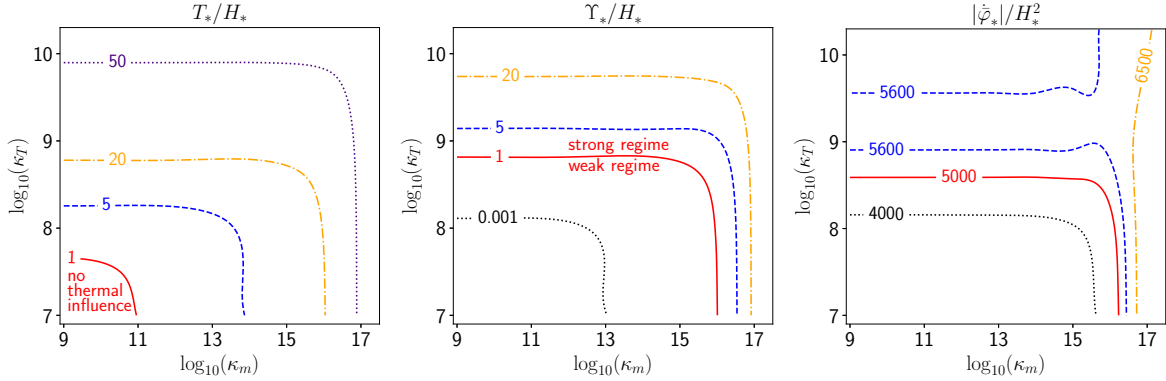


Figure 4: The main physical characteristics of the background solution at the “freeze-out point”, $k_*/(aH) \equiv 1$, as a function of the parameters κ_m and κ_T parametrizing Υ (cf. eq. (5.1)). Left: the temperature T , normalized to the Hubble rate H . Middle: like at left, but for the friction coefficient Υ . The “strong” and “weak” regime, as well as the corner where the thermal plasma has no influence, refer to item (i) in sec. 2.2. Right: the inflaton derivative, $\dot{\phi}$, normalized to H^2 . Even if the value does not vary much, the variation has a non-trivial shape, which correlates in an intriguing way with curvature perturbations (cf. the text).

6. Can $\mathcal{P}_{\mathcal{R}}$ be expressed in terms of freeze-out parameters?

In the case of normal “cold” inflation, to which our setup reduces if $\Upsilon, T \ll H$, it is well known that the out-of-horizon power spectrum, $\mathcal{P}_{\mathcal{R}}(k \ll aH)$, can be approximated (within a few percent accuracy) by

$$\mathcal{P}_{\mathcal{R}}^{\text{vac}} \equiv \frac{H_*^4}{(2\pi\dot{\phi}_*)^2}, \quad (6.1)$$

where $f_* \equiv f(t_*)$ denotes the value of $f(t)$ evaluated at the time $t = t_*$ when the pivot scale exits the Hubble horizon, i.e. $k_* \equiv a(t_*)H(t_*)$. In warm inflation literature, it is generally assumed that the presence of fluctuations and dissipation modifies eq. (6.1) through a function which depends on the values of the medium-induced quantities at the freeze-out point, normalized to the corresponding Hubble rate, notably T_*/H_* and Υ_*/H_* (cf. eqs. (6.2) and (6.3)). We refer to these ratios as *freeze-out parameters*.

An immediate remark is that, as is visible in eq. (6.1), we should consider $|\dot{\phi}_*|/H_*^2$ as an additional freeze-out parameter. In fact, $\dot{\phi}^2$ plays a prominent role in eqs. (2.14) and (2.15). In phenomenological scans, the value of $|\dot{\phi}_*|/H_*^2$ varies by many orders of magnitude (cf. table 1 on p. 26). However, the way that we have organized the scans of the present section, by keeping the potential fixed (cf. appendix A), implies that $|\dot{\phi}_*|/H_*^2$ only varies by $\mathcal{O}(1)$ (cf. fig. 4). This simplifies our task of identifying possible functional dependences.

The values of the freeze-out parameters T_*/H_* , Υ_*/H_* and $|\dot{\phi}_*|/H_*^2$ are shown in fig. 4. The similar shapes of the contours of constant T_*/H_* and Υ_*/H_* suggest that these parameters

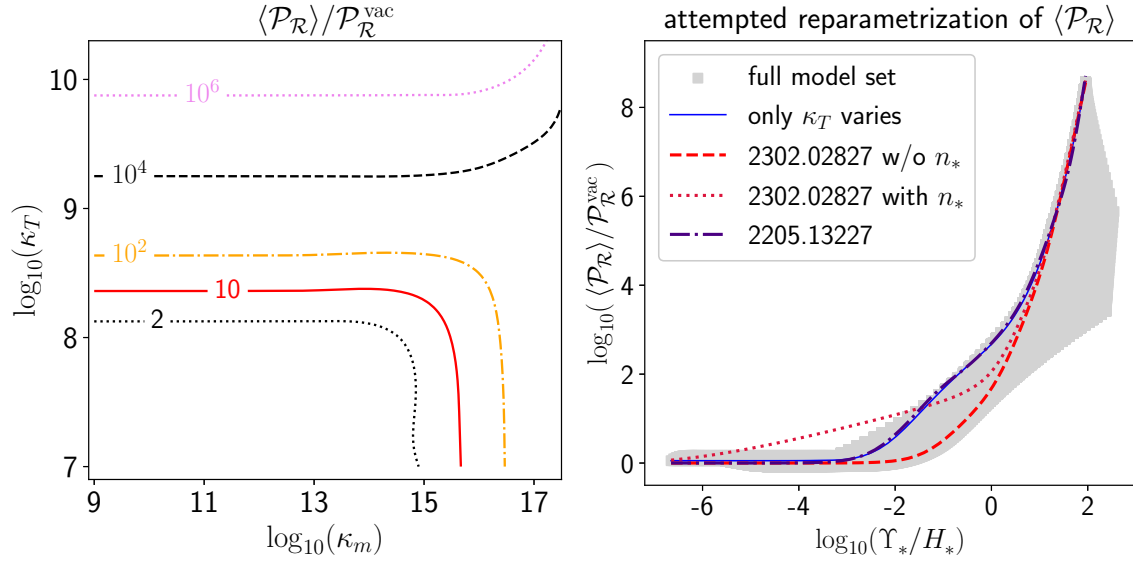


Figure 5: Left: $\langle \mathcal{P}_{\mathcal{R}} \rangle / \mathcal{P}_{\mathcal{R}}^{\text{vac}}$ outside of the Hubble horizon, $k_*/(aH) \equiv 10^{-5}$, as a function of κ_m and κ_T parametrizing Υ (cf. eq. (5.1)). Right: $\langle \mathcal{P}_{\mathcal{R}} \rangle / \mathcal{P}_{\mathcal{R}}^{\text{vac}}$ replotted versus the freeze-out parameter Υ_*/H_* from fig. 4(middle). We also compare a specific model (“only κ_T varies”, implying $\Upsilon \sim T^3$) with fit forms from the literature (cf. the text). The grey band shows that $\langle \mathcal{P}_{\mathcal{R}} \rangle$ is *not* a single-valued function of $Q_* = \Upsilon_*/(3H_*)$, but displays a large spread as Q_* increases.

are strongly correlated. The contours of constant $|\dot{\varphi}_*|/H_*^2$ show a different shape, particularly in the strong regime, however the variation is mild.

The key question is whether $\mathcal{P}_{\mathcal{R}}$ respects the shapes of the curves of constant freeze-out parameters. The value $\log_{10}(\langle \mathcal{P}_{\mathcal{R}} \rangle / \mathcal{P}_{\mathcal{R}}^{\text{vac}})$ is plotted in fig. 5(left). Clearly, the curves do *not* display the same geometry as the contours of constant T_*/H_* and Υ_*/H_* in fig. 4. They resemble more those of constant $|\dot{\varphi}_*|/H_*^2$, even if only qualitatively.

To be more concrete, we denote $Q_* \equiv \Upsilon_*/(3H_*)$, and recall two ansätze for $\langle \mathcal{P}_{\mathcal{R}} \rangle$ from warm inflation literature,

$$\langle \mathcal{P}_{\mathcal{R}} \rangle \stackrel{[8], \text{eq. (4.26)}}{\equiv} \frac{\overbrace{H_*^4}^{\equiv \mathcal{P}_{\mathcal{R}}^{\text{vac}}}}{(2\pi\dot{\varphi}_*)^2} \left(1 + \frac{\overbrace{2\theta_*}^{\equiv 2n_*}}{e^{H_*/T_*} - 1} + \frac{2\sqrt{3}\pi Q_*}{\sqrt{3 + 4\pi Q_*}} \frac{T_*}{H_*} \right) \mathcal{G}(Q_*) \quad (6.2)$$

$$\stackrel{[16], \text{eq. (49)}}{\equiv} \frac{H_*^4}{(2\pi\dot{\varphi}_*)^2} \left[1 + \frac{12Q_* T_* F_2(3Q_*)}{H_*} \right], \quad (6.3)$$

where, according to ref. [8], $\theta_* = 1$ if φ is thermalized, otherwise $\theta_* = 0$.⁴ Obviously, eqs. (6.2) and (6.3) can always be postulated if the result depends on a single parameter,

⁴The inclusion of $2n_*$ was questioned in ref. [18]. The origin of this factor can be seen in eq. (3.21). As shown in eq. (3.30), when we match quantum mechanics to the classical Langevin description, the Bose distribution appears through the noise autocorrelator. The linear T_* dependence, visible in eqs. (6.2) and

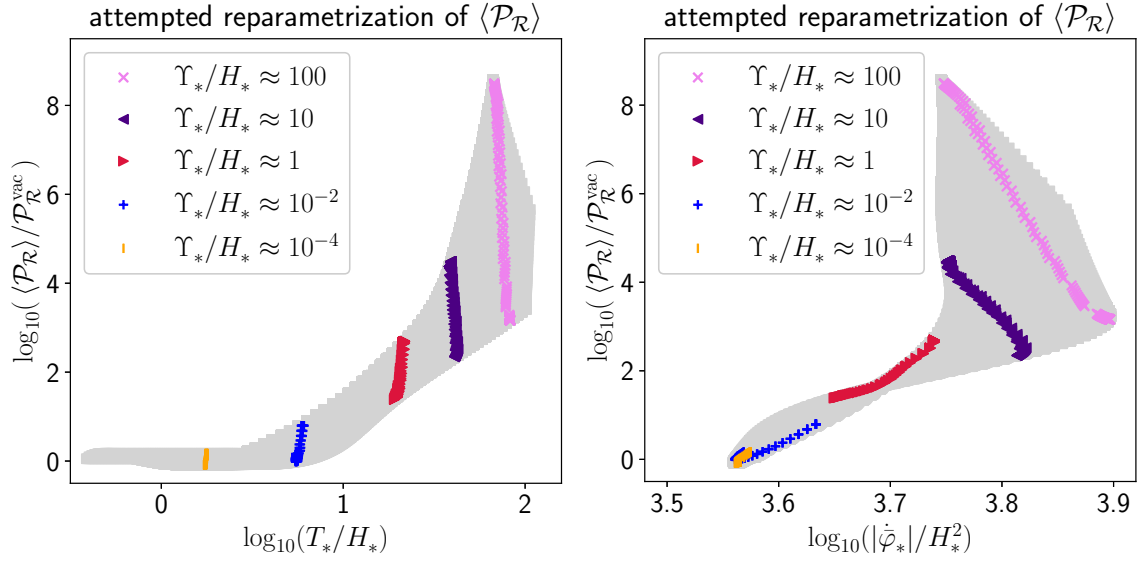


Figure 6: $\langle \mathcal{P}_{\mathcal{R}} \rangle$ from fig. 5(left), replotted versus the freeze-out parameters T_*/H_* and $|\dot{\varphi}_*|/H_*^2$ from fig. 4. The left panel shows that the multi-valuedness of $\langle \mathcal{P}_{\mathcal{R}} \rangle / \mathcal{P}_{\mathcal{R}}^{\text{vac}}$ is *not* efficiently resolved by including T_*/H_* as an additional freeze-out parameter: the chosen subsets are almost vertical in T_*/H_* . The right panel shows that results vary noticeably with $|\dot{\varphi}_*|/H_*^2$, however this is partly an optical illusion, as we have zoomed into a very narrow range of values. Nevertheless, it is interesting that the sign of the correlation switches between $\Upsilon_*/H_* = 1$ and 10, when the radiation energy density overtakes the inflaton kinetic energy, $e_r > \dot{\varphi}^2/2$.

with the function \mathcal{G} or F_2 adjusted to capture the parameter dependence. The non-trivial question is if such a representation could be *model-independent*, like the vacuum limit in eq. (6.1), which applies to any potential V and any momentum k (whether close to the pivot scale or not, and whether matched to CMB data or not). Let us anticipate that we find the answer to be negative, and do *not* make use of eq. (6.2) or (6.3) in our own analysis, however we compare with them for a particular single-parameter family of variations (cf. fig. 5(right)).

Now, physical intuition might suggest that the final result *should be* a function of the freeze-out parameters. The simplest way to say this is that a classical thermal state has no memory. All its properties should be fixed by a few macroscopic control parameters, as they appear in the evolution equations. Evidence for a certain degree of universality was put forward in ref. [19]. It was demonstrated that \mathcal{G} is independent of the φ -dependence of Υ , the inflaton potential V , and the number of e -folds (or the momentum k). Also, it was stated that it does not matter if Q evolved or is treated as constant (though most of the runs kept it time-independent). At the same time, significant non-universality was observed between

(6.3), is a special kinematic limit of n_{B} , cf. eq. (3.31). In our approach, n_{B} appears nowhere else than the noise autocorrelator, and the thermalization or not of φ is determined by the dynamics.

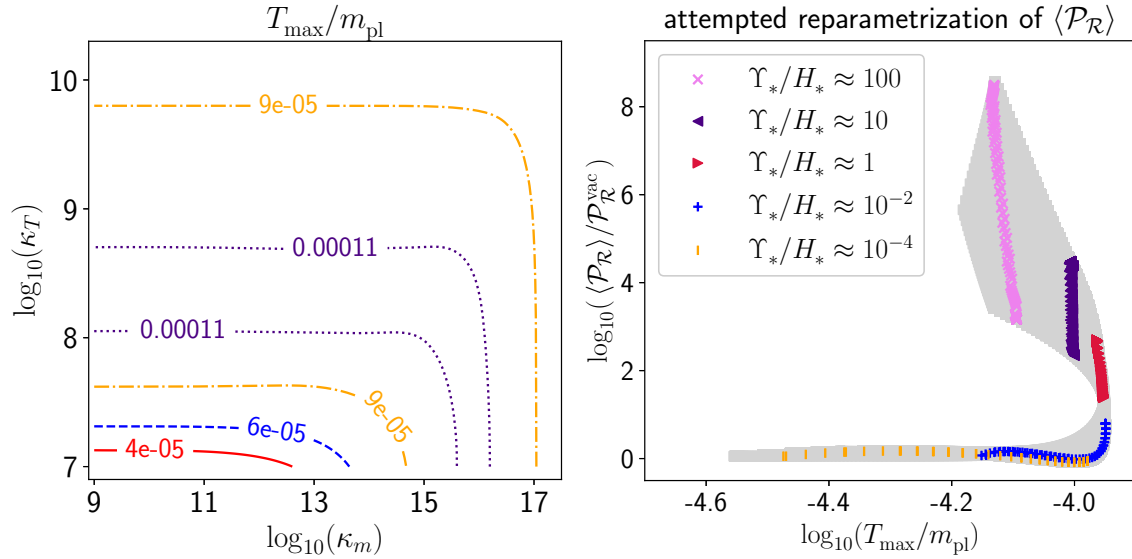


Figure 7: Left: the maximal temperature reached during the reheating history, as a function of the parameters κ_m and κ_T parametrizing Υ (cf. eq. (5.1)). Even though Υ varies by many orders of magnitude, T_{\max} only varies modestly. Right: an attempted reparametrization of $\langle \mathcal{P}_{\mathcal{R}} \rangle$ from fig. 5(left), versus T_{\max} . We observe that in the weak regime, $\langle \mathcal{P}_{\mathcal{R}} \rangle / \mathcal{P}_{\mathcal{R}}^{\text{vac}}$ is practically independent of T_{\max} , whereas in the strong regime, the value of Υ_*/H_* effectively fixes that of T_{\max}/m_{pl} , so that the latter *cannot* resolve the model dependence (vertical variation) in a natural way.

models with different T -dependences of Q .

We can scrutinize numerically the universality of the curvature power spectrum. Our tool is that the scans in sec. 6 span a two-parameter set of models. We can then replace the original parameters through the would-be freeze-out parameters. We replot the scan results from fig. 5(left) as a function of various freeze-out parameters in figs. 5(right) and 6.

As a first test, the solid blue line in fig. 5(right) shows the result obtained if we keep κ_m fixed to its minimum, $\kappa_m = 10^9$, and only let κ_T vary. Then, effectively, $\Upsilon \sim T^3$, a case that has been studied in the literature (cf., e.g., ref. [30]). We show a comparison with employing eq. (4.27) of ref. [8] in eq. (6.2) [“2302.02827”], and eq. (47) of ref. [16] in eq. (6.3) [“2205.13227”]. Our results agree well with ref. [16].

Our main diagnostics is shown in fig. 6. In the left panel, we highlight subsets with a specific Υ_*/H_* , as a function of T_*/H_* . However, the sets remain practically vertical: trajectories of constant Υ_*/H_* correspond to constant T_*/H_* , so that T_*/H_* has no resolving power.

In contrast, the right panel of fig. 6 shows the dependence on $|\dot{\varphi}_*|/H_*^2$, revealing a correlation. Notably, in the weak regime, $\langle \mathcal{P}_{\mathcal{R}} \rangle / \mathcal{P}_{\mathcal{R}}^{\text{vac}}$ grows with $|\dot{\varphi}_*|/H_*^2$, whereas in the strong regime, it decreases. However, in both cases, $|\dot{\varphi}_*|/H_*^2$ only varies very little, so we cannot represent an orders-of-magnitude change of $\langle \mathcal{P}_{\mathcal{R}} \rangle / \mathcal{P}_{\mathcal{R}}^{\text{vac}}$ in any natural way (e.g. a power).

To summarize, a large model dependence remains present in the power spectrum, if we try to capture the results by only making use of the freeze-out parameters T_*/H_* and Υ_*/H_* . We have seen indications, however, that additional freeze-out parameters, perhaps involving the energy densities $\dot{\bar{\varphi}}_*^2/2$ and e_r , could help to capture the model dependence. Unfortunately, given the complicated structure of the coupled evolution equations (2.13)–(2.15), we have not been able to identify analytically the precise quantities that could take this role.

To end this section, we show a different correlation, not with freeze-out parameters but with the maximal temperature reached during the evolution (T_{\max}). Its value in the plane of κ_m and κ_T is plotted in fig. 7(left); compared with T_*/H_* in fig. 4(left), the shape is quite different. An attempted reparametrization of $\langle \mathcal{P}_{\mathcal{R}} \rangle / \mathcal{P}_{\mathcal{R}}^{\text{vac}}$ in terms of T_{\max}/m_{pl} is illustrated in fig. 7(right). Even though we again observe a geometrically interesting correlation, and a very clear difference between the weak and strong regimes, the plot does not suggest any natural way to resolve the degeneracy in both regimes. It is also appropriate to remark that in some cases, notably in the model considered in sec. 7, the temperature does not peak, but is rather a slowly decreasing function during the reheating epoch.

7. Testing a Standard Model embedded warm inflation scenario

As a second application, we consider a Standard Model embedded warm inflation scenario, recently proposed in ref. [31] (subsequently also considered in ref. [32]). The inflaton potential and the friction coefficient, which we adopt at face value from ref. [31], read

$$V(\bar{\varphi}) \equiv \lambda \bar{\varphi}^4, \quad \text{for } |\bar{\varphi}| \gg \text{GeV}, \quad (7.1)$$

$$\Upsilon(\bar{\varphi}, T) \equiv \frac{T^2}{2f_a^2} \left[\frac{1}{\alpha_s^5 N_c^5 T} + \frac{2N_f}{N_c H(\bar{\varphi}, T)} \right]^{-1}, \quad N_c \equiv 3, \quad N_f \equiv 5. \quad (7.2)$$

For the three parameters (λ , f_a and α_s), we consider the same values as in ref. [31], as well as small variants of f_a , as tabulated in table 1. The background evolution is started with a common field value, large enough to cover all sets, $\bar{\varphi}(t_{\text{ref}}) \equiv \bar{\varphi}_{\text{ref}} \equiv 7 m_{\text{pl}}$, at a time

$$t_{\text{ref}} \equiv \sqrt{\frac{3}{8\pi}} \frac{m_{\text{pl}}}{\sqrt{V(\bar{\varphi}_{\text{ref}})}}. \quad (7.3)$$

The initial time derivative $\dot{\bar{\varphi}}(t_{\text{ref}})$ and temperature T_{ref} are fixed in analogy with eqs. (A.3) and (A.6), respectively. The time t_1 at which $k_*/(aH) = 10^2$ and we start evolving the perturbations, has been determined from a match to Standard Model thermodynamics, as explained around eq. (5.2).

The observables that we compute are the mean value of the scalar amplitude,

$$A_s \equiv \langle \mathcal{P}_{\mathcal{R}}(k_*, t) \rangle_{k_*/(aH)=10^{-5}}, \quad (7.4)$$

original input [2503.18829v2]			our output							
λ	f_a [10^{12} GeV]	α_s	t_1/t_{ref}	$\bar{\varphi}_1/m_{\text{pl}}$	T_*/H_*	Q_*	$ \dot{\bar{\varphi}} _*/H_*^2$	A_s	n_s	r
10^{-21}	0.146	0.0269	7417	1.03	8042	14.9	1.14p8	2.73m9	0.967	1.46m11
10^{-20}	0.264	0.0263	4310	1.26	3660	9.25	3.01p7	2.70m9	0.969	3.39m10
10^{-19}	0.518	0.0257	2121	1.67	1527	4.85	7.22p6	2.07m9	0.968	1.35m8
10^{-18}	1.05	0.0251	954	2.27	601	2.21	1.66p6	1.93m9	0.968	4.93m7
10^{-17}	2.30	0.0246	373	3.18	211	0.687	3.65p5	2.03m9	0.967	1.80m5
10^{-16}	4.95	0.0243	178	4.07	61.6	0.0951	8.40p4	2.15m9	0.971	4.62m4
10^{-15}	8.69	0.0242	148	4.36	19.8	0.0134	2.32p4	1.85m9	0.980	7.15m3

adjusted input			our output							
λ	f_a [10^{12} GeV]	α_s	t_1/t_{ref}	$\bar{\varphi}_1/m_{\text{pl}}$	T_*/H_*	Q_*	$ \dot{\bar{\varphi}} _*/H_*^2$	A_s	n_s	r
10^{-21}	0.153	0.0269	6897	1.06	7798	13.9	1.11p8	2.11m9	0.968	2.12m11
10^{-20}	0.278	0.0263	3969	1.31	3534	8.59	2.91p7	2.09m9	0.970	5.00m10
10^{-19}	0.516	0.0257	2135	1.67	1531	4.88	7.24p6	2.11m9	0.969	1.31m8
10^{-18}	1.025	0.0251	994	2.24	618	2.30	1.69p6	2.10m9	0.968	4.27m7
10^{-17}	2.27	0.0246	381	3.15	213	0.711	3.68p5	2.10m9	0.967	1.68m5
10^{-16}	4.98	0.0243	177	4.08	60.9	0.0919	8.38p4	2.09m9	0.971	4.79m4
10^{-15}	8.56	0.0242	149	4.35	20.4	0.0150	2.33p4	2.09m9	0.980	6.26m3

Table 1: The original [31] (top panel) and adjusted (bottom panel) parameters for a scenario defined by the potential and friction coefficient in eqs. (7.1) and (7.2), respectively. Here t_1 is the time at which $k_*/(aH) = 10^2$ and we start evolving perturbations; t_{ref} is defined in eq. (7.3) and agrees in order of magnitude with the inverse of the initial Hubble rate; the freeze-out parameters are evaluated when $k_*/(aH) = 1$; and A_s , n_s , r are evaluated when $k_*/(aH) = 10^{-5}$. We employ the shorthand notation $mX \equiv 10^{-X}$, $pX \equiv 10^{+X}$. The most stringent observational constraint originates from the spectral tilt, $n_s = 0.974 \pm 0.003$ [1, 2].

as well as other quantities that can be derived from it, notably the spectral tilt,

$$n_s - 1 \equiv \left. \frac{d \ln \langle \mathcal{P}_{\mathcal{R}}(k_*, t) \rangle}{d \ln k} \right|_{k_*/(aH)=10^{-5}} \approx \frac{\log_{10} \langle \mathcal{P}_{\mathcal{R}}(10^{+\delta} k_*, t) \rangle - \log_{10} \langle \mathcal{P}_{\mathcal{R}}(10^{-\delta} k_*, t) \rangle}{2\delta}. \quad (7.5)$$

The subtraction results in significance loss, implying that δ cannot be taken arbitrarily small; a value $\delta \sim 0.1$ is large enough for clear variation, but not so large that $\mathcal{O}(\delta^2)$ matters. In addition to A_s and n_s , we also evaluate the ratio of tensor and scalar power spectra,

$$r \equiv \frac{\mathcal{P}_t}{A_s}, \quad \mathcal{P}_t \approx \frac{16H_*^2}{\pi m_{\text{pl}}^2}. \quad (7.6)$$

The tensor spectrum gets a contribution from thermal noise, but it grows as k^3 [33–35], and

is hence small in the CMB domain of very small k . Therefore, it is reasonable to employ the vacuum prediction for the tensor spectrum, as indicated in eq. (7.6).

In the top panel of table 1, we employ the same input parameters as in ref. [31]. We then find A_s somewhat different from the CMB value $A_s \approx 2.10 \times 10^{-9}$. One cause for this could be the model dependence discussed in sec. 6 (ref. [31] employed a fit from ref. [16], valid for $\Upsilon \sim T^3$, even though eq. (7.2) has a different form).

On the other hand, as shown in the bottom panel of table 1, by adjusting f_a modestly, we can tune A_s to agree with observation. The corresponding n_s is within $\sim 2\sigma$ of current data (though it displays some differences compared with ref. [31]). At this confidence level, we confirm the viability of the model proposed in ref. [31].

8. Conclusions and outlook

Given the growing interest in the physics of density perturbations at shorter length scales (larger momenta) than is relevant for the CMB, we have developed a framework for computing their evolution across a smooth reheating period. For this, it has been important to avoid the approximations adopted, if only CMB physics is of interest (cf. sec. 2). The purpose of the present study has been to implement this framework in its full domain of validity, which requires the inclusion of thermal fluctuations. To incorporate quantum aspects, we have derived the noise autocorrelator through a matching to quantum-statistical physics deep inside the Hubble horizon (cf. sec. 3). We have also shown that the gauge-invariant stochastic equations can be studied numerically with standard methods (cf. sec. 4).

In addition to reheating, our framework can also be employed in the context of warm inflation. Apart from comparing with recent literature, whose fit forms have been employed in model building (cf. fig. 5(right)), we have scrutinized the “universality” of power spectra that originate from warm inflation. To offer a new angle on this topic, we have explored a two-parameter non-powerlaw family of friction coefficients (cf. eq. (5.1)), motivated by the functional form arising from its microscopic derivation for sphaleron heating. The two parameters give us sufficient freedom to meaningfully test the premise of universality.

Our results show that the model dependence of $\langle \mathcal{P}_{\mathcal{R}} \rangle$ *cannot* be hidden by reparametrizing the result in terms of T_*/H_* and $Q_* \equiv \Upsilon_*/(3H_*)$ (cf. fig. 6(left)). On the other hand, the introduction of $\dot{\varphi}_*/H_*^2$ could offer possibilities for this (cf. fig. 6(right)). However, $\dot{\varphi}_*/H_*^2$ appears in a complicated way in the evolution equations (cf. eqs. (2.13)–(2.15)), and the dynamics it affects is subtle, as \mathcal{R}_φ decouples in the limit where the φ energy density is subdominant [6] (during inflation only the milder hierarchy $\dot{\varphi}^2 \ll e_r$ can be realized). Therefore, we have not been able to identify a simple freeze-out parameter that could hide the model dependence, though we do not consider it impossible that such a parameter exists.

As a second application, we have tested the recent proposal of ref. [31] of embedding warm

inflation within the Standard Model. Even if we find small differences, requiring a modest adjustment of one of the input parameters (cf. table 1), and even if our spectral tilt n_s is larger in the weak regime, the qualitative features of the solutions found in ref. [31] can be confirmed. In particular, our n_s is consistent with current CMB data [1,2] at the 2σ level.

To summarize, the tests carried out show that by adopting a more complete framework than has been the norm in the warm inflation context (avoiding gauge fixing and slow-roll approximations, and extrapolating thermal noise self-consistently towards the quantum domain $k/a \geq T$), one can eliminate theoretical doubts without inducing additional numerical cost. Hopefully, in the future, we can use this framework to tackle our original main goal, the study of scalar-induced gravitational waves originating from the reheating epoch.

Acknowledgements

We thank Sebastian Zell for helpful discussions and valuable comments on the manuscript.

A. Inflaton potential, radiation plasma, and background initial conditions

The benchmarks and scans of secs. 5 and 6 focus on understanding the physics originating from the damping coefficient Υ and the thermal noise ϱ , so it is helpful to fix the vacuum potential and the initial conditions, guaranteeing that not too many parameters vary simultaneously. For the potential we choose the ansatz referred to as “natural inflation” [36],

$$V(\bar{\varphi}) \equiv m^2 f_a^2 \left[1 - \cos\left(\frac{\bar{\varphi}}{f_a}\right) \right], \quad (\text{A.1})$$

with the parameter values

$$f_a = 1.25 m_{\text{pl}}, \quad m = 1.09 \times 10^{-6} m_{\text{pl}}. \quad (\text{A.2})$$

For $(\Upsilon/H)(k_*) \ll 1.0$, these yield a curvature power spectrum $\mathcal{P}_{\mathcal{R}}(k_*) \approx 2.1 \times 10^{-9}$, in good agreement with CMB data. The initial conditions are taken as

$$\bar{\varphi}(t_{\text{ref}}) = 3.5 m_{\text{pl}}, \quad \dot{\bar{\varphi}}(t_{\text{ref}}) = -\frac{V_{,\varphi}(3.5 m_{\text{pl}})}{3H_{\text{ref}} + \Upsilon_{\text{ref}}}, \quad (\text{A.3})$$

where the initial time and its inverse are defined as

$$t_{\text{ref}} \equiv \sqrt{\frac{3}{4\pi}} \frac{m_{\text{pl}}}{m \bar{\varphi}(t_{\text{ref}})}, \quad H_{\text{ref}} \equiv t_{\text{ref}}^{-1}. \quad (\text{A.4})$$

The value of $\bar{\varphi}(t_{\text{ref}})$ implies that we start near the top of V , and $\dot{\bar{\varphi}}(t_{\text{ref}})$ ensures that we soon approach the slow-roll trajectory. However, $H_{\text{ref}} \neq H(t_{\text{ref}})$, and therefore the solution displays an initial transient. Afterwards, a period of quasi de Sitter expansion follows, with $\dot{H} \ll H^2$. The initial conditions have been chosen “conservatively”, in the sense that, for large Υ , the solution undergoes hundreds of e -folds, before we reach the time $t = t_1$, at which we start evolving the perturbations (cf. fig. 1(left)). Horizon exit takes place soon afterwards.

Turning to the properties of the radiation plasma, it is represented by the energy density and pressure

$$e_r = \frac{g_* \pi^2 T^4}{30}, \quad p_r = \frac{g_* \pi^2 T^4}{90}, \quad g_* = 106.75, \quad (\text{A.5})$$

where the value of g_* is chosen so that the late-time dynamics can be matched onto a Standard Model plasma. The initial condition for T needs to be fixed and, even if the exact choice does not matter, transients can be reduced by searching for an approximate stationary temperature following from eq. (2.18),

$$(e_r + p_r)(T_{\text{ref}}) = \frac{\Upsilon_{\text{ref}} \dot{\bar{\varphi}}^2(t_{\text{ref}})}{3H_{\text{ref}}}, \quad (\text{A.6})$$

where $T_{\text{ref}} \equiv T(t_{\text{ref}})$ and $\Upsilon_{\text{ref}} \equiv \Upsilon(T_{\text{ref}})$.

References

- [1] N. Aghanim *et al* [Planck], *Planck 2018 results. VI. Cosmological parameters*, Astron. Astrophys. 641 (2020) A6; *ibid.* 652 (2021) C4 (erratum) [1807.06209].
- [2] T. Louis *et al.*, *The Atacama Cosmology Telescope: DR6 Power Spectra, Likelihoods and Λ CDM Parameters*, [2503.14452].
- [3] A. Andrews *et al.* [Euclid], *Euclid: Field-level inference of primordial non-Gaussianity and cosmic initial conditions*, [2412.11945].
- [4] P. Parashari and R. Laha, *Primordial power spectrum in light of JWST observations of high redshift galaxies*, Mon. Not. Roy. Astron. Soc. 526 (2023) L63 [2305.00999].
- [5] N. Aggarwal *et al.*, *Challenges and opportunities of gravitational-wave searches at MHz to GHz frequencies*, Living Rev. Rel. 24 (2021) 4 [2011.12414].
- [6] M. Laine, S. Procacci and A. Rogelj, *Evolution of coupled scalar perturbations through smooth reheating. Part I. Dissipative regime*, JCAP 10 (2024) 040 [2407.17074].
- [7] A. Berera, *The Warm Inflation Story*, Universe 9 (2023) 272 [2305.10879].
- [8] V. Kamali, M. Motaharfar and R.O. Ramos, *Recent developments in warm inflation*, Universe 9 (2023) 124 [2302.02827].
- [9] C. Graham and I.G. Moss, *Density fluctuations from warm inflation*, JCAP 07 (2009) 013 [0905.3500].
- [10] M. Bastero-Gil, A. Berera and R.O. Ramos, *Shear viscous effects on the primordial power spectrum from warm inflation*, JCAP 07 (2011) 030 [1106.0701].
- [11] R.O. Ramos and L.A. da Silva, *Power spectrum for inflation models with quantum and thermal noises*, JCAP 03 (2013) 032 [1302.3544].
- [12] M. Bastero-Gil, A. Berera, I.G. Moss and R.O. Ramos, *Cosmological fluctuations of a random field and radiation fluid*, JCAP 05 (2014) 004 [1401.1149].
- [13] J. Yokoyama and A.D. Linde, *Is warm inflation possible?*, Phys. Rev. D 60 (1999) 083509 [hep-ph/9809409].
- [14] W. DeRocco, P.W. Graham and S. Kalia, *Warming up cold inflation*, JCAP 11 (2021) 011 [2107.07517].
- [15] T. Fujita, K. Mukaida and T. Tsuji, *Reheating after Axion Inflation*, [2503.01228].
- [16] M. Mirbabayi and A. Gruzinov, *Shapes of non-Gaussianity in warm inflation*, JCAP 02 (2023) 012 [2205.13227].
- [17] G. Ballesteros, M.A.G. García, A. Pérez Rodríguez, M. Pierre and J. Rey, *Primordial black holes and gravitational waves from dissipation during inflation*, JCAP 12 (2022) 006 [2208.14978].
- [18] G. Ballesteros, A. Pérez Rodríguez and M. Pierre, *Monomial warm inflation revisited*, JCAP 03 (2024) 003 [2304.05978].

- [19] G. Montefalcone, V. Aragam, L. Visinelli and K. Freese, *WarmSPy: a numerical study of cosmological perturbations in warm inflation*, JCAP 01 (2024) 032 [2306.16190].
- [20] M. Mirbabayi, *Loosely coupled particles in warm inflation*, JCAP 05 (2025) 067 [2409.17927].
- [21] G.S. Rodrigues and R.O. Ramos, *WI2easy: warm inflation dynamics made easy*, [2504.17760].
- [22] E. Broadberry, A. Hook and S. Mondal, *Warm Inflation with Pseudo-scalar couplings*, [2505.07943].
- [23] H. Kolesova, M. Laine and S. Procacci, *Maximal temperature of strongly-coupled dark sectors*, JHEP 05 (2023) 239 [2303.17973].
- [24] M. Laine and S. Procacci, *Minimal warm inflation with complete medium response*, JCAP 06 (2021) 031 [2102.09913].
- [25] D. Bödeker and J. Nienaber, *Scalar field damping at high temperatures*, Phys. Rev. D 106 (2022) 056016 [2205.14166].
- [26] K. Bouzoud and J. Ghiglieri, *Thermal axion production at hard and soft momenta*, JHEP 01 (2025) 163 [2404.06113].
- [27] M. Laine, L. Niemi, S. Procacci and K. Rummukainen, *Shape of the hot topological charge density spectral function*, JHEP 11 (2022) 126 [2209.13804].
- [28] S. Zell, *No Warm Inflation From Sphaleron Heating With a Vanilla Axion*, [2408.07746].
- [29] M. Laine, M. Meyer and Y. Schröder, *Data for the Standard Model equation of state*, <http://laine.itp.unibe.ch/eos15/>.
- [30] K.V. Berghaus, P.W. Graham and D.E. Kaplan, *Minimal warm inflation*, JCAP 03 (2020) 034; *ibid.* 10 (2023) E02 (erratum) [1910.07525].
- [31] K.V. Berghaus, M. Drewes and S. Zell, *Warm Inflation with the Standard Model*, [2503.18829].
- [32] R.O. Ramos and G.S. Rodrigues, *Viability of warm inflation with standard model interactions*, Phys. Rev. D 111 (2025) 123527 [2504.20943].
- [33] Y. Qiu and L. Sorbo, *The spectrum of tensor perturbations in warm inflation*, Phys. Rev. D 104 (2021) 083542 [2107.09754].
- [34] P. Klose, M. Laine and S. Procacci, *Gravitational wave background from vacuum and thermal fluctuations during axion-like inflation*, JCAP 12 (2022) 020 [2210.11710].
- [35] G. Montefalcone, B. Shams Es Haghi, T. Xu and K. Freese, *Thermal Gravitons from Warm Inflation*, [2507.08739].
- [36] K. Freese, J.A. Frieman and A.V. Olinto, *Natural inflation with pseudo Nambu-Goldstone bosons*, Phys. Rev. Lett. 65 (1990) 3233.